# Deglacial upslope shift of NE Atlantic intermediate waters controlled slope erosion and cold-water coral mound formation (Porcupine Seabight, Irish margin)

Claudia Wienberg, Jürgen Titschack, Norbert Frank, Ricardo de Pol-Holz, Jan Fietzke, Markus Eisele, Anne Kremer, Dierk Hebbeln

HAL Id: hal-02971186

https://hal.science/hal-02971186

Submitted on 16 Apr 2021

# Deglacial upslope shift of NE Atlantic intermediate waters controlled slope erosion and cold-water coral mound formation (Porcupine Seabight, Irish margin)

Claudia Wienberg [a, *], Jürgen Titschack [a, b], Norbert Frank [c, d], Ricardo De Pol-Holz [e], Jan Fietzke [f], Markus Eisele [a], Anne Kremer [a], Dierk Hebbeln [a]

[a] MARUM - Center for Marine Environmental Sciences, University of Bremen, Leobener Strasse 8, 28359, Bremen, Germany
[b] Senckenberg am Meer (SaM), Marine Research Department, Südstrand 40, 26382, Wilhelmshaven, Germany
[c] Institute of Environmental Physics (IUP), Heidelberg University, Im Neuenheimer Feld 229, 69120 Heidelberg, Germany
[d] Laboratoire des Sciences du Climat et de l'Environnement (LSCE), Bat.12, Avenue de la Terrasse, 91198, Gif-sur-Yvette, France
[e] Centro de Investigación GAIA-Antártica (CIGA), Universidad de Magallanes, Av. Bulnes 01855, 6210427, Punta Arenas, Chile
[f] GEOMAR - Helmholtz Center for Ocean Research Kiel, Wischhofstr. 1-3, 24148, Kiel, Germany

## ARTICLE INFO

## ABSTRACT

Turbulent bottom currents significantly influence the formation of cold-water coral mounds and sedimentation processes on continental slopes. Combining records from coral mounds and adjacent slope sediments therefore provide an unprecedented palaeo-archive to understand past variations of intermediate water-mass dynamics. Here, we present coral ages from coral mounds of the Belgica province (Porcupine Seabight, NE Atlantic), which indicate a non-synchronous Holocene re-activation in mound formation suggested by a temporal offset of ~2.7 kyr between the deep (start: ~11.3 ka BP at 950 m depth) and shallow (start: ~8.6 ka BP at 700 m depth) mounds. A similar depth-dependent pattern is revealed in the slope sediments close to these mounds that become progressively younger from 22.1 ka BP at 990 m to 12.2 ka BP at 740 m depth (based on core-top ages). We suggest that the observed changes are the consequence of enhanced bottom-water hydrodynamics, caused by internal waves associated to the re-invigoration of the Mediterranean Outflow Water (MOW) and the development of a transition zone (TZ) between the MOW and the overlying Eastern North Atlantic Water (ENAW), which established during the last deglacial. These highly energetic conditions induced erosion adjacent to the Belgica mounds and supported the re-initiation of mound formation by increasing food and sediment fluxes. The striking depth-dependent patterns are likely linked to a shift of the ENAW-MOW-TZ, moving the level of maximum energy ~250 m upslope since the onset of the last deglaciation.

## 1. Introduction

Intermediate water masses are often associated with turbulent bottom-currents that shape the seafloor along continental slopes by erosion, transport and selective deposition of sediments (Cacchione et al., 2002; Dickson and McCave, 1986; García et al., 2009; Rebesco et al., 2014; Shanmugam, 2017). In particular internal waves, propagating along the pycnocline between two water masses and breaking on slopes, are important sources of hydrodynamic energy at mid-depths (~200−1000 m; Vic et al., 2019).

They move stratified waters up and down a sloping surface and create turbulence of sufficient energy to erode and transport sediments (Cacchione et al., 2002; Pomar et al., 2012). The erosive effect of internal waves locally results in low sedimentation rates or even non-deposition on continental slopes (Lim et al., 2010; Pomar et al., 2012), impeding the reconstruction of palaeo-environmental conditions (e.g., Erdem et al., 2016; Titschack et al., 2009). Accordingly, there is a lack of records, that allow us to decipher past variations in mid-depths hydrodynamics in full temporal resolution.

Turbulent hydrodynamics related to internal waves also play a vital role in forming benthic habitats, as they sustain the benthic faunal community by mobilizing food (Frederiksen et al., 1992; Lim et al., 2018; Mohn et al., 2014). Enhanced bottom shear-stress

induced by internal waves causes high levels of suspended material that lead to the formation of nepheloid layers, which enrich the availability of food for benthic communities living within or below this layer (Cacchione and Drake, 1986; Mienis et al., 2007). In addition, by moving waters up and down the slope, internal waves enhance the lateral transport of particulate organic matter and hence support substantially the supply of food to sessile organisms (e.g., Duineveld et al., 2007; Hebbeln et al., 2016; Lim et al., 2018; Monteiro et al., 2005; Mosch et al., 2012; Rice et al., 1990).

Important marine ecosystems occurring widespread on the upper continental slopes (<1000 m) in the North Atlantic Ocean are cold-water coral (CWC) mounds (Roberts et al., 2006; Wienberg and Titschack, 2017). The formation of coral mounds depends on the sustained growth of scleractinian CWCs and a contemporaneous regular supply of sediments, and mound deposits consists of almost equal contents of coral fragments and hemipelagic sediments (e.g., Titschack et al., 2009). Coral growth and sediment supply are closely linked to the dynamic flow of intermediate water masses (Frank et al., 2011; Henry et al., 2014) and internal-tide-related high energetic conditions (Cyr et al., 2016; Mohn et al., 2014). These secure the delivery of high amounts of food and sediment particles, which support CWC growth and maintain mound formation, respectively (Hebbeln et al., 2016). The skeletal frameworks of the scleractinian CWCs play thereby a critical role as they baffle suspended sediments from the bottom waters and provide accommodation space for the deposition of these sediments in an otherwise erosive setting (Huvenne et al., 2009; Titschack et al., 2009). Coral mounds develop over geological timescales (millennia and more; e.g., Kano et al., 2007), yet their formation is discontinuous and stratigraphic records are marked by unconformities often associated to long-lasting hiatuses (corresponding to a temporary stagnation in mound formation) (e.g., Dorschel et al., 2005; López Correa et al., 2012; Matos et al., 2017; Raddatz et al., 2014; Victorero et al., 2016; Wienberg et al., 2018). Nevertheless, coral mounds represent unique palaeo-archives as the preserved mound sediment sequences (corresponding to periods of mound formation) display a high stratigraphical resolution (Bonneau et al., 2018; Frank et al., 2009; Wefing et al., 2017). Moreover, they record oceanographic and environmental changes primarily during times of high energetic bottom-current conditions, while adjacent slope areas are concurrently affected by non-deposition or erosion (De Haas et al., 2009; Thierens et al., 2013; Titschack et al., 2009). Consequently, the combination of palaeo-records from coral mounds and adjacent slope areas (see also Hebbeln et al., 2019b) offer great potential to trace and understand past variations in mid-depth hydrodynamics and their impact on slope sedimentation and marine habitats.

Following this approach, we present data obtained from coral mounds and slope sediments of the prominent Belgica coral mound province (CMP) in the Porcupine Seabight off Ireland (Fig. 1). The coral mounds of this CMP are arranged in two chains that stretch from north to south parallel to the slope (Fig. 1B; Beyer et al., 2003). The formation of two mound chains that follow distinct depth contours (700 and 950 m) was likely the result of past vertical variations of the intermediate water column structure, as it has already been suggested for other Atlantic CMPs comprising water-depth-dependent mound chains (e.g., off Morocco and Mauritania; Hebbeln et al., 2019a; Wienberg et al., 2018). However, while it is well-known that the Late Quaternary development of the Belgica mounds responded to a climate-related pattern with mound formation being constrained to interglacial periods (e.g., Frank et al., 2011), limited knowledge exists on inter-mound variability in particular on differences in mound development between both chains. Focussing on the latest mound formation period during the

Holocene, we present ~50 new coral datings from the Belgica CMP, which allow for the first time to decipher any short-term (centennial to millennial) variations in mound formation between both mound chains during the last ~11 kyr. In addition, sediment cores collected along a depth transect close to the Belgica mounds (Fig. 1) demonstrate the relationship between coral-mound aggradation and sedimentation pattern in adjacent slope areas. By combining the records from these two archives, coral mounds and slope sediments, this study sheds new light on the dynamics of intermediate water masses in the NE Atlantic in time and space.

## 2. Study area

### 2.1. Belgica coral mound province

The Porcupine Seabight off Ireland is a hotspot area for the occurrence of coral mounds (Fig. 1A). Here, more than 1000 exposed and buried coral mounds are grouped into provinces, such as the Magellan, Hovland, and Belgica CMPs (e.g., Beyer et al., 2003; De Mol et al., 2002; Huvenne et al., 2007; Wheeler et al., 2007). The prominent and well-studied Belgica CMP is on the eastern slope of the Porcupine basin and comprises ~35 large coral mounds (Fig. 1B) with mean heights of 100 m above the seafloor (total height range: 40−160 m; Beyer et al., 2003; Wheeler et al., 2007). They are arranged in two north-south-trending chains (Fig. 1B; Beyer et al., 2003) with the majority of the mounds rising from the ~750 m (shallow mound chain) and 900−950 m (deep mound chain) depth contours, while their summits mainly occur in 700 m and 800−850 m water depth, respectively (a detailed geomorphological description of the Belgica CMP is presented by Wheeler et al., 2007). In addition to the large Belgica mounds, hundreds of very small mound structures (Moira mounds) with heights of less than 10 m occur in 800-1100 m water depth between the two mound chains and west of the deep mounds (Lim et al., 2017; Wheeler et al., 2005, 2011). It is speculated that they are of Holocene age (Foubert et al., 2011; Huvenne et al., 2005), though this assumption is mainly based on their size and has not confirmed by definitive dating.

In contrast, much effort has been conducted to decipher the temporal development of the large Belgica mounds. A unique stratigraphic record exists for the Challenger mound (shallow mound chain; Fig. 1B), which was drilled down to its base in ~155 m below seafloor during IODP Expedition 307 (Ferdelman et al., 2006; Williams et al., 2006) and allowed to date the timing of mound initiation back to ~2.6−2.7 Ma (Huvenne et al., 2009; Kano et al., 2007). This timing in mound initiation is valid for the majority of coral mounds along the Irish margin as most of them root on one common seismic reflector (Van Rooij et al., 2003). The Challenger mound record revealed a first period of almost continuous mound formation between the Early to Mid-Pleistocene (~2.7−1.6 Ma; Kano et al., 2007). Following a major hiatus, the formation of Challenger mound re-initiated at 0.8 Ma after the mid-Pleistocene transition. Its Late Quaternary development is characterised by a discontinuous mound formation, which responded to a climate-related pattern with mound formation being mainly constrained to interglacials (Frank et al., 2009; Kano et al., 2007; Raddatz et al., 2014). This pattern of predominant interglacial mound formation was also observed for core records from mounds of the deep Belgica mound chain (Galway and Thérèse mounds; Eisele et al., 2008; Frank et al., 2009; van der Land et al., 2014) as well as for other CMPs of the Porcupine Seabight and the Rockall Through (Bonneau et al., 2018; De Haas et al., 2009; Dorschel et al., 2005, Dorschel et al., 2007b; Frank et al., 2009; Mienis et al., 2009; Rüggeberg et al., 2007; Victorero et al., 2016). The youngest period in mound
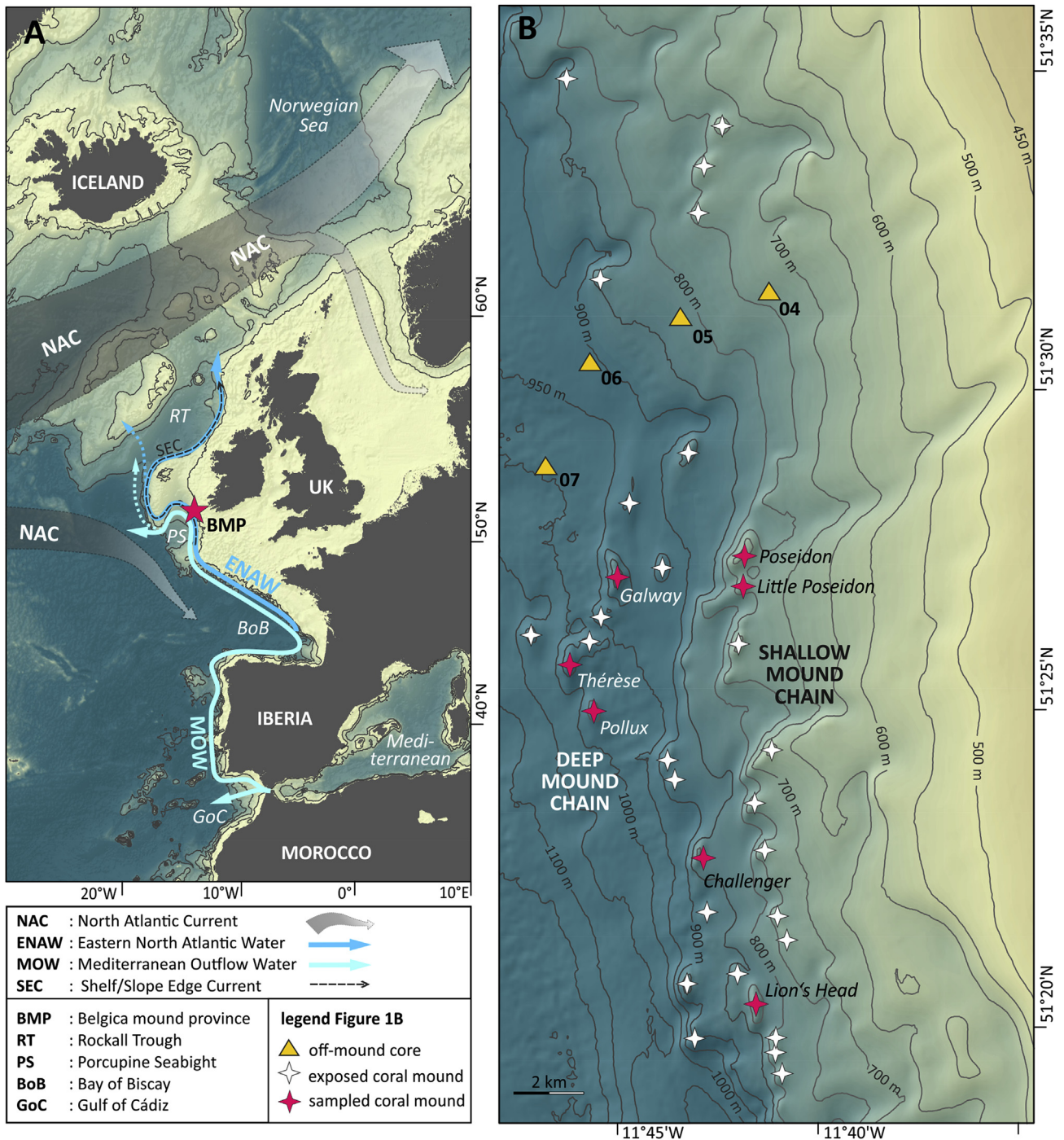
**Fig. 1.** A Overview map showing the NE Atlantic with main features of its present-day mid-depth oceanography (see legend for abbreviations). B Detailed map (contour interval: 50 m) showing the distribution of exposed coral mounds (white and pink stars, the latter marking coral mounds being considered for this study) within the Belgica coral mound province on the eastern mid-slope of the Porcupine Seabight (modified after Andersen et al., 2010; Beyer et al., 2003, 2006). Off-mound sediment cores collected along a depth transect between 740 and 990 m are indicated (yellow triangles; core-ID: GeoB145xx). (For interpretation of the references to colour in this figure legend, the reader is referred to the Web version of this article.)

formation commenced with the onset of the Holocene and persists until today (e.g., Frank et al., 2011). Nevertheless, beside the broadly accepted climate change-driven pattern, major knowledge gaps still exist with respect to variations in mound formation on shorter (centennial to millennial) timescales, which are mainly attributed to the limited number of coral ages (Supplementary Material: see Table S1 for a compilation of coral ages of the Belgica CMP). For example, for the youngest Holocene mound formation period only

20 coral ages are available for the Belgica CMP (see Table 1 for references), which are not sufficient to examine any temporal variability in mound formation between both chains (see also Wienberg and Titschack, 2017). This Holocene age data set is even more biased as the coral ages mainly originate from the deep Belgica mounds (n= 14; see Table 1 for references).

Today, the deep Belgica mounds (e.g., Thérèse and Galway mounds; Fig. 1B) host the most vivid coral communities in the area,

**Table 1**

Metadata of cold-water coral-bearing sediment material collected from various coral mounds of the Belgica coral mound province (PO: Poseidon, LP: Little Poseidon, LH: Lion's Head, CH: Challenger, GA: Galway, TH: Thérèse, PX: Pollux; for position see Fig. 1B). Number of U-series (U/Th) and AMS radiocarbon ($^{14}$C) coral datings is indicated, which were either obtained during this study or previously published (1: Schröder-Ritzrau et al., 2005, 2: Raddatz et al., 2014, 3a: Frank et al., 2005, 3b: Frank et al., 2009, 3c: Frank et al., 2011, 4: Eisele et al., 2008, 5: Van der Land et al., 2014). The number of Holocene coral ages for each sampling site is given in bold, while the total number of ages is given in brackets. M: coral mound, LAT: latitude, LON: longitude, WD: water depth, REC: core recovery, GC: gravity core; DC: drill core; GR: grab sample; DR: dredge sample.

| M | Sample-ID | Gear | LAT (N) | LON (W) | WD (m) | REC (m) | Location on mound | $^{14}$C | U/Th | Reference |
|---|---|---|---|---|---|---|---|---|---|---|
| **shallow coral mound chain** | | | | | | | | | | |
| PO | GeoB 14535-2 | GR | 51°27.33′ | 11°42.18′ | 675 | bulk | top | **6** (7) | | this study |
| | GeoB 14546-1 | GC | 51°27.64′ | 11°41.95′ | 699 | 1.70 | flank | **2** (2) | | this study |
| | GeoB 14547-1 | GC | 51°27.48′ | 11°41.88′ | 681 | 4.28 | top | | **1** (1) | this study |
| | GeoB 14550-1 | GC | 51°27.33′ | 11°42.18′ | 676 | 5.58 | top | **1** (1) | **0** (1) | this study |
| | 3140 | DR | 51°27.20′ | 11°42.20′ | 681 | bulk | / | | **1** (1) | 1 |
| LP | GeoB 14539-1 | GR | 51°26.90′ | 11°42.98′ | 686 | bulk | top | **8** (8) | | this study |
| CH | IODP1317 | DC | 51°23′ | 11°43′ | 800 | 16.0 | / | | **1** (15) | 2 |
| | MD01-2451G | GC | 51°23′ | 11°43′ | 762 | 12.8 | top | | **4** (7) | 3a & 3b |
| LH | GeoB 14511-1 | GR | 51°20.39′ | 11°41.64′ | 707 | bulk | top | **8** (8) | | this study |
| | GeoB 14518-1 | GC | 51°20.38′ | 11°41.64′ | 707 | 5.87 | top | **1** (1) | **5** (5) | this study |
| | GeoB 14519-1 | GC | 51°20.33′ | 11°41.76′ | 794 | 3.97 | flank | | **0** (2) | this study |
| **deep coral mound chain** | | | | | | | | | | |
| GA | GeoB 9212-1 | GC | 51°27.13′ | 11°44.99′ | 847 | 1.93 | flank | **1** (1) | | this study |
| | GeoB 9213-1 | GC | 51°27.09′ | 11°45.16′ | 793 | 5.15 | top | **1** (1) | **3** (3) | this study |
| | | | | | | | | **1** (1) | **1** (4) | 4 & 5 |
| | GeoB 9214-1 | GC | 51°27.06′ | 11°45.28′ | 857 | 4.89 | flank | **1** (1) | | this study |
| | | | | | | | | **2** (2) | **2** (4) | 4 & 5 |
| | GeoB 9223-1 | GC | 51°26.90′ | 11°45.10′ | 839 | 4.63 | flank | **1** (1) | **0** (2) | 4 & 5 |
| TH | MD01-2463G | GC | 51°26′ | 11°46′ | 888 | 10.8 | top | **2** (2) | **3** (16) | 3a & 3c |
| PX | GeoB 14530-1 | GC | 51°24.89′ | 11°45.82′ | 950 | 5.08 | flank | **1** (1) | **2** (3) | this study |
| | GeoB 14531-1 | GC | 51°24.89′ | 11°45.77′ | 904 | 4.49 | top | **1** (1) | **4** (4) | this study |
| | GeoB 14532-2 | GC | 51°24.88′ | 11°45.62′ | 926 | 1.03 | flank | | **3** (3) | this study |
| | 2419 & 2420 | DR | 51°24.80′ | 11°45.90′ | 1005 | bulk | / | | **2** (2) | 1 |

*Note: total number of coral ages available for the Belgica coral mound province: this study: $n_{Holocene} = 49$; published in 1−5: $n_{Holocene} = 20$).

dominated by *Lophelia pertusa* (recently synonymised to *Desmophyllum pertusum*; Addamo et al., 2016) and *Madrepora oculata*, with living corals occurring mainly on the mound summits (De Mol et al., 2007; Dorschel et al., 2007a; Foubert et al., 2005). In contrast, the summits of the shallow mounds (e.g., Challenger mound) are widely covered by coral rubble and dead coral framework (Foubert et al., 2005). However, new video observations showed that isolated live coral colonies are also found on the current-facing flanks of some shallow mounds (e.g. Poseidon and Little Poseidon mounds), and even numerous live colonies of *L. pertusa* and *M. oculata* were detected on the top of Lion's Head mound, which is situated in the southern part of the shallow mound chain (Fig. 1B; Wienberg et al., 2010).

### 2.2. Oceanographic setting

The intermediate water masses that influence the Belgica mounds in the Porcupine Seabight are the Eastern North Atlantic Water (ENAW; ~200−700 m water depth), the Mediterranean Outflow Water (MOW; ~700-1400 m water depth), and the Labrador Sea Water (LSW; ~1400-1,800m; Fig. 2) (van Aken, 2000). The ENAW comprises a mixture of subpolar and subtropical gyre waters. As part of the southern branch of the North Atlantic Current (NAC), it flows into the Bay of Biscay (Fig. 1A), where it experiences intense deep winter mixing (Pingree, 1993; van Aken and Becker, 1996). A substantial portion of the ENAW is carried northwards by the shelf or slope edge currents (SEC; Fig. 1A), which is a prominent feature of the mid-slope circulation within the Porcupine Seabight and the Rockall Trough (Huthnance, 1986; Pingree and LeCann, 1990; White, 2007).

MOW originates from the Mediterranean Sea (Millot, 2014) and is marked by a salinity maximum (Fig. 2) and an oxygen minimum at ~950 m depth (Pollard et al., 1996). After exiting the Strait of Gibraltar, the MOW settles at intermediate depths and flows as a significant contour current north-westward along the Iberian middle slope (Hernández-Molina et al., 2014; Serra et al., 2010). It splits into two branches of different densities (upper and lower MOW, centred at 500−800 m and at 1000−1400 m depth, respectively), whose flow pathways are mainly controlled by the seafloor topography in the Gulf of Cádiz (Baringer and Price, 1999; Johnson et al., 2002; Rogerson et al., 2012b). The lower MOW flows further west towards the open ocean basin, while the upper MOW advects northwards (Baringer and Price, 1999; Bower et al., 2002; Reid, 1979). Its northward flow is linked to an along-slope (geostrophic) current system that originates at the Iberian margin (Fig. 1A), though the northward penetration of MOW shows temporal variability due to the expansion and contraction of the subpolar gyre in response to variable wind strength (Lozier and Stewart, 2008). The LSW is a cold water mass with a relatively low salinity compared to the overlying MOW (Fig. 2). It is formed in the Labrador Sea and transported into the NE Atlantic by the deep North Atlantic Current (NAC; Fig. 1) (Paillet et al., 1998).

Within the Porcupine Seabight, a permanent pycnocline is developed at the interface of the ENAW and the MOW, which forms a diffusive transition zone (TZ) between 700 and 900 m water depth (Fig. 2; Dickson and McCave, 1986; Dullo et al., 2008; White and Dorschel, 2010). The ENAW-MOW-TZ is marked by a longer persistence of particles (including organic matter) forming nepheloid layers (Dickson and McCave, 1986). A strong residual near-seabed current flow with highest current speeds (>15 cm s$^{-1}$) is associated with the pycnocline and energy supply is further enhanced by turbulent mixing induced by internal waves and tides (Dickson and McCave, 1986; Mohn et al., 2014; White, 2007; White and Dorschel, 2010). The dynamic conditions induced by geostrophic currents and internal waves promote significant along-slope sediment transport and provide large across-slope sediment movement and organic matter fluxes (Rice et al., 1991; White and Dorschel, 2010). The intense bottom-current activity significantly
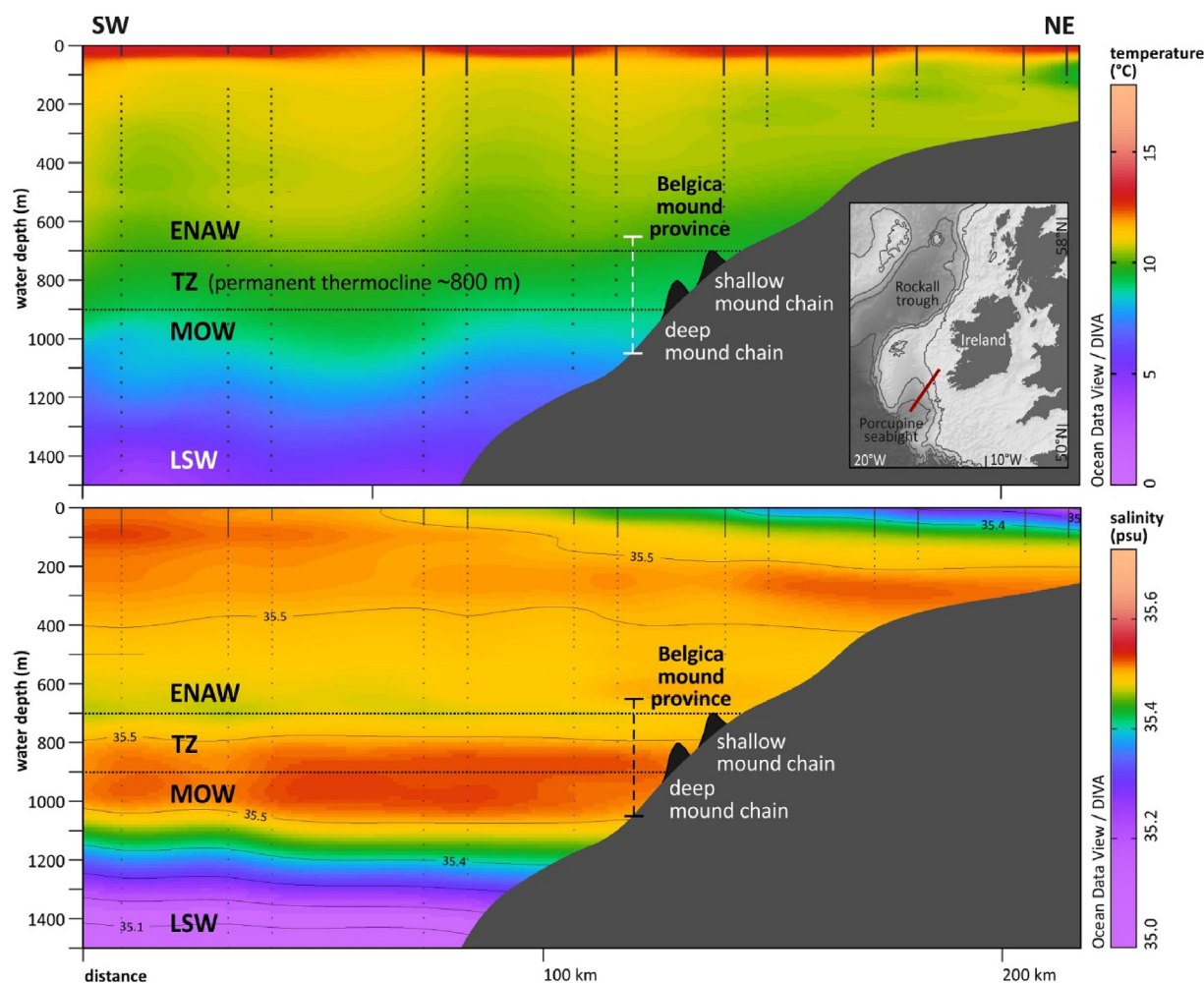
**Fig. 2.** Depth-temperature (upper graph) and depth-salinity profile (lower graph) across the eastern slope of the Porcupine Seabight (data source: WOA13 (Locarnini et al., 2013; Zweng et al., 2013); generated with ODV v5.1.5, R. Schlitzer 2018; red line in the overview map indicates the position of the NE-SW cross-profile). The temperature and salinity data clearly show the Eastern North Atlantic Water (ENAW) overlying the Mediterranean Outflow Water (MOW) with its salinity maximum at ~950 m water depth. Below the MOW flows the Labrador Sea Water (LSW), which is colder and has a reduced salinity compared to the MOW. The boundary between the ENAW and MOW is marked by a permanent thermocline and comprises a rather broad transition zone (TZ) between 700 and 900 m water depth. The shallow and deep coral mound chains of the Belgica province occurring within the ENAW-MOW-TZ are indicated. The total depth range of coral mound occurrences (650−1050 m; considering summits and bases of the mounds) is marked by the dashed (white/black) bar. (For interpretation of the references to colour in this figure legend, the reader is referred to the Web version of this article.)

shapes the seafloor in the Porcupine Seabight. The Belgica mounds are enclosed by drift sediments and up to 50-m-deep moats have developed at their steep western downslope flanks (Van Rooij et al., 2003). In addition, the widespread occurrence of topographical features, such as barchan dunes, gravel ridges, and sediment waves, found close to the mounds further indicates that the slope area today is affected by a highly turbulent bottom-current regime (Dorschel et al., 2007a; Foubert et al., 2005; Huvenne et al., 2005; Wheeler et al., 2005). Bottom-current data obtained from Galway mound (deep mound chain; Fig. 1B) revealed poleward flowing geostrophic currents, almost perpendicular tidal currents, and a maximum current speed of 51 cm s$^{-1}$ at the mound summit (Dorschel et al., 2007a).

## 3. Material and methods

The sediment material analysed for this study was collected during R/V Poseidon expedition POS400 ("CORICON") in 2010 (Wienberg et al., 2010) and during R/V Meteor expedition M61-3 in 2004 (Ratmeyer and cruise participants, 2006). Thirteen on-mound

gravity cores (defined as sediment cores bearing varying contents of coral fragments) and three coral-containing grab samples were selected to extend the existing coral stratigraphy of the Belgica mounds, which were collected from the summits and flanks of different coral mounds of both mound chains (Table 1; Fig. 1). The on-mound cores have recoveries between 103 and 587 cm (Table 1) and are composed of varying contents of CWC fragments (mainly *L. pertusa* and *M. oculata*) embedded in hemipelagic sediments. From all sediment cores and grab samples, CWC fragments were selected for dating. In addition, during expedition POS400, four off-mound gravity cores (defined as sediment cores barren of any CWC fragments) were collected in the northern part of the Belgica CMP adjacent to the coral mounds along a water depth transect of ~740−990 m (Fig. 1). The off-mound cores show core recoveries between 480 and 550 cm and are composed of fine-grained (silty clay to clayey silt) hemipelagic sediments with occasional drop-stones (Table 2). Radiocarbon datings supported by X-ray fluorescence (XRF) data-based core-to-core correlations were used to establish age models for these off-mound cores.

**Table 2**
Metadata of coral-barren 'off-mound' sediment cores collected during R/V Poseidon cruise P400. The cores were retrieved in the northern part of the Belgica coral mound province adjacent to exposed corals mounds and comprise a depth transect between ~740 and 990 m. Analyses conducted on these cores are indicated (XRF: X-ray fluorescence scans, [14]C: AMS radiocarbon dating).

| Core-ID | Latitude | Longitude | Water depth | Recovery | XRF | [14]C | Remarks |
|---------|----------|-----------|-------------|----------|-----|-------|---------|
| | (N) | (W) | (m) | (cm) | | | |
| GeoB 14504-1 | 51°31.54′ | 11°41.96′ | 739 | 499 | X | 4 | ./. |
| GeoB 14505-1 | 51°31.03′ | 11°43.85′ | 832 | 540 | X | 2 | 0−1 cm: dropstone |
| GeoB 14506-1 | 51°30.27′ | 11°45.89′ | 911 | 550 | X | 3 | ./. |
| GeoB 14507-1 | 51°28.53′ | 11°47.02′ | 987 | 476 | X | 2 | 127 cm: dropstone |

### 3.1. AMS radiocarbon and uranium-series dating on cold-water coral fragments

Well-preserved fragments of the framework-forming species *L. pertusa* and *M. oculata* were sampled at various core depths from the coral-bearing on-mound sediment cores and from the bulk grab samples listed in Table 1. Coral fragments were either used for accelerator mass spectrometry (AMS) radiocarbon (^{14}C) age determination or for Uranium-series dating. Prior to analyses, all coral fragments were cleaned mechanically to remove contaminants (borings by organisms, iron−manganese crusts, coatings) from the fossil skeleton surfaces according to a procedure described by Frank et al. (2004).

Radiocarbon dating was performed at the BETA Analytic (Miami, Florida, USA) and at the Leibniz Laboratory for Radiometric Dating and Stable Isotope Research at the Christian-Albrechts-University (Kiel, Germany). All AMS ^{14}C ages of CWCs were corrected for ^{13}C and calibrated using the CALIB7.1 software (Stuiver and Reimer, 1993). For the calibration, we have applied the MARINE13 calibration curve (Reimer et al., 2013) with a local reservoir age correction $\Delta R$ of $100 \pm 100$ years accounting for the observation of a Holocene thermocline reservoir age of $R = 480 \pm 120$ years by Frank et al. (2004, 2005). All radiocarbon ages are reported as kiloyears before 1950 AD (abbreviated as ka BP; Table 3).

Uranium-series measurements were performed at the Laboratoire des Sciences du Climat et de l'Environnement (LSCE, Gif-sur-Yvette, France) using a quadrupole inductively coupled plasma mass spectrometry (Q-ICP-MS) (Douville et al., 2010), at the

**Table 3**
AMS radiocarbon (^{14}C) dates obtained from cold-water coral fragments collected from coral mounds of the Belgica coral mound province (PO: Poseidon, LP: Little Poseidon, LH: Lion's Head, GA: Galway, PX: Pollux; for position see Fig. 1B). The AMS ^{14}C ages were corrected for ^{13}C and calibrated using the CALIB7.1 software (Stuiver and Reimer, 1993). For the calibration, we have applied the MARINE13 calibration curve (Reimer et al., 2013) with a local reservoir age correction $\Delta R$ of $100 \pm 100$ years accounting for the observation of a Holocene thermocline reservoir age of $R = 480 \pm 120$ years by Frank et al. (2004, 2005). M: coral mound, GC: gravity core, GR: grab sample, SD: sampling depth, COR: coral species, Mo: *Madrepora oculata*, Lp: *Lophelia pertusa*, CalAR: calibrated age range, CalAge: calibrated average age (rounded).

| No. | M | Sample-ID | Gear | SD | COR | Labcode | [14]C age | 1σ | 2σ (95.4%) CalAR | | CalAge | ± (2σ) |
|-----|---|-----------|------|----|-----|---------|-----------|-----|------------------|---|--------|--------|
| | | (GeoB) | | (cm) | | | (ka BP, P = AD 1950) | | | | | |
| **shallow coral mound chain** | | | | | | | | | | | | |
| 1 | PO_top | 14535−2 | GR | 0 | Mo | BETA 344871 | 1.730 | 0.03 | 951 | 1.377 | 1.160 | 0.210 |
| 2 | PO_top | 14535−2 | GR | 0 | Lp | BETA 344869 | 2.060 | 0.03 | 1.295 | 1.761 | 1.530 | 0.230 |
| 3 | PO_top | 14535−2 | GR | 0 | Mo | BETA 344870 | 2.120 | 0.03 | 1.344 | 1.828 | 1.590 | 0.240 |
| 4 | PO_top | 14535−2 | GR | 0 | Lp | BETA 340739 | 2.170 | 0.03 | 1.391 | 1.883 | 1.640 | 0.250 |
| 5 | PO_top | 14535−2 | GR | 0 | Mo | BETA 340737 | 4.380 | 0.03 | 4.085 | 4.704 | 4.390 | 0.310 |
| 6 | PO_top | 14535−2 | GR | 0 | Mo | BETA 344868 | 8.090 | 0.04 | 8.202 | 8.729 | 8.470 | 0.260 |
| 7 | PO_flank | 14546−1 | GC | 3 | Mo | BETA 340743 | 0.910 | 0.03 | 0.259 | 0.620 | 0.440 | 0.180 |
| 8 | PO_flank | 14546−1 | GC | 58 | Lp | BETA 340744 | 7.250 | 0.03 | 7.434 | 7.827 | 7.630 | 0.200 |
| 9 | PO_top | 14550−1 | GC | 6 | Lp | BETA 340745 | 7.480 | 0.03 | 7.619 | 8.040 | 7.830 | 0.210 |
| 10 | LP_top | 14539−1 | GR | 0 | Lp | BETA 340740 | 3.370 | 0.03 | 2.832 | 3.356 | 3.090 | 0.260 |
| 11 | LP_top | 14539−1 | GR | 0 | Lp | BETA 344874 | 3.880 | 0.03 | 3.444 | 3.989 | 3.720 | 0.270 |
| 12 | LP_top | 14539−1 | GR | 0 | Lp | BETA 340742 | 6.980 | 0.03 | 7.196 | 7.571 | 7.380 | 0.190 |
| 13 | LP_top | 14539−1 | GR | 0 | Mo | BETA 344873 | 7.200 | 0.04 | 7.401 | 7.797 | 7.600 | 0.200 |
| 14 | LP_top | 14539−1 | GR | 0 | Mo | BETA 344876 | 7.210 | 0.03 | 7.409 | 7.804 | 7.610 | 0.200 |
| 15 | LP_top | 14539−1 | GR | 0 | Mo | BETA 340741 | 7.240 | 0.03 | 7.600 | 7.811 | 7.620 | 0.200 |
| 16 | LP_top | 14539−1 | GR | 0 | Mo | BETA 344872 | 7.460 | 0.04 | 7.685 | 8.021 | 7.810 | 0.210 |
| 17 | LP_top | 14539−1 | GR | 0 | Mo | BETA 344875 | 7.550 | 0.04 | 7.925 | 8.139 | 7.910 | 0.230 |
| 18 | LH_top | 14511−1 | GR | 0 | Mo | BETA 344865 | 0.600 | 0.04 | 0.001 | 0.331 | 0.170 | 0.170 |
| 19 | LH_top | 14511−1 | GR | 0 | Mo | BETA 340732 | 0.830 | 0.03 | 0.128 | 0.536 | 0.330 | 0.200 |
| 20 | LH_top | 14511−1 | GR | 0 | Mo | BETA 344863 | 0.830 | 0.03 | 0.128 | 0.536 | 0.330 | 0.200 |
| 21 | LH_top | 14511−1 | GR | 0 | Mo | BETA 344862 | 0.880 | 0.03 | 0.227 | 0.616 | 0.420 | 0.190 |
| 22 | LH_top | 14511−1 | GR | 0 | Mo | BETA 340731 | 1.030 | 0.03 | 0.327 | 0.684 | 0.510 | 0.180 |
| 23 | LH_top | 14511−1 | GR | 0 | Mo | BETA 344866 | 1.160 | 0.03 | 0.473 | 0.832 | 0.650 | 0.180 |
| 24 | LH_top | 14511−1 | GR | 0 | Mo | BETA 344864 | 1.500 | 0.03 | 0.723 | 1.157 | 0.950 | 0.230 |
| 25 | LH_top | 14511−1 | GR | 0 | Mo | BETA 340733 | 1.770 | 0.03 | 0.974 | 1.430 | 1.200 | 0.230 |
| 26 | LH_top | 14518−1 | GC | 33 | Mo | BETA 340734 | 2.680 | 0.03 | 1.975 | 2.570 | 2.270 | 0.300 |
| **deep coral mound chain** | | | | | | | | | | | | |
| 27 | GA_flank | 9212−1 | GC | 63 | ? | KIA 31268 | 3.330 | 0.04 | 2.784 | 3.318 | 3.050 | 0.270 |
| 28 | GA_top | 9213−1 | GC | 13 | Mo | BETA 340729 | 3.230 | 0.03 | 2.714 | 3.191 | 2.950 | 0.240 |
| 29 | GA_flank | 9214−1 | GC | 20 | Lp | BETA 340730 | 1.430 | 0.00 | 0.666 | 1.096 | 0.880 | 0.220 |
| 30 | PX_flank | 14530−1 | GC | 180 | Lp | BETA 340735 | 6.060 | 0.03 | 6.177 | 6.624 | 6.400 | 0.220 |
| 31 | PX_top | 14531−1 | GC | 207 | Lp | BETA 340736 | 5.920 | 0.03 | 5.978 | 6.451 | 6.210 | 0.240 |

KIA: Leibniz Laboratory for Radiometric Dating at the Christian-Albrechts-University (Kiel, Germany).
BETA: BETA Analytic (Miami, Florida, USA).

**Table 4**

Uranium-series (calculated) ages obtained from cold-water coral fragments collected from coral mounds of the Belgica coral mound province (PO: Poseidon, LH: Lion's Head, GA: Galway, PX: Pollux; for position see Fig. 1B). Supplemented are $^{232}$Th concentrations and decay corrected $^{234}$U/$^{238}$U activity ratios ($\delta^{234}$U(i); calculated from the given ages and with $\lambda^{234}$U: $2.8263 \times 10^{-6}$ yr$^{-1}$). Note: 22 ages are reliable (R) with $\delta^{234}$U(i) values of $146.8 \pm 10$‰ (modern seawater; Andersen et al., 2010); 11 ages ranging between 200 and 650 ka BP are unreliable and only presented in the Supplementary Material. M: coral mound, GC: gravity core, CD: core depth, COR: coral species, Mo: *Madrepora oculata*, Lp: *Lophelia pertusa*.

| No. | M | Sample ID (GeoB) | Gear | CD (cm) | COR | Labcode | $^{232}$Th (ppb) | ± (ppb) | $\delta^{234}$U(i) (‰) | ± (‰) | Age (ka BP) | ± (ka) | |
|---|---|---|---|---|---|---|---|---|---|---|---|---|---|
| **shallow coral mound chain** | | | | | | | | | | | | | |
| 1 | PO$_{top}$ | 14547−1 | GC | 3 | Mo | GEOMAR | 5.179 | 0.003 | 142.3 | | 7.887 | 0.03 | R |
| 2 | PO$_{top}$ | 14550−1 | GC | 35 | Lp | GEOMAR | 16.334 | 0.025 | 148.4 | | 252.907 | 3.07 | R |
| 3 | LH$_{top}$ | 14518−1 | GC | 3 | Mo | GIF 3063 | 0.389 | 0.001 | 147.3 | 1.5 | 0.284 | 0.03 | R |
| 4 | LH$_{top}$ | 14518−1 | GC | 64 | Mo | GIF 3051 | 0.329 | 0.001 | 148.7 | 1.5 | 4.134 | 0.04 | R |
| 5 | LH$_{top}$ | 14518−1 | GC | 98 | Mo | GIF 3052 | 0.663 | 0.001 | 148.8 | 1.5 | 6.430 | 0.05 | R |
| 6 | LH$_{top}$ | 14518−1 | GC | 150 | Lp | IUPH6142 | 0.334 | 0.005 | 147.3 | 3.8 | 7.747 | 0.16 | R |
| 7 | LH$_{top}$ | 14518−1 | GC | 155 | Mo | GIF 3053 | 0.471 | 0.001 | 151.1 | 1.5 | 8.556 | 0.06 | R |
| 8 | LH$_{flank}$ | 14519−1 | GC | 49 | Lp | GIF 3071 | 13.377 | 0.037 | 152.0 | 2.1 | 98.158 | 0.10 | R |
| 9 | LH$_{flank}$ | 14519−1 | GC | 136 | Lp | GIF 3072 | 0.379 | 0.001 | 157.5 | 2.3 | 139.476 | 0.99 | R |
| **deep coral mound chain** | | | | | | | | | | | | | |
| 10 | GA$_{top}$ | 9213−1 | GC | 51 | Lp | GIF 3058 | 0.287 | 0.001 | 150.1 | 1.5 | 5.628 | 0.04 | R |
| 11 | GA$_{top}$ | 9213−1 | GC | 104 | Lp | GIF 3059 | 0.252 | 0.001 | 148.6 | 1.5 | 6.577 | 0.05 | R |
| 12 | GA$_{top}$ | 9213−1 | GC | 250 | Lp | GIF 3060 | 0.875 | 0.001 | 150.3 | 1.5 | 9.195 | 0.07 | R |
| 13 | PX$_{flank}$ | 14530−1 | GC | 19 | Lp | GIF 3065 | 0.516 | 0.001 | 148.4 | 1.5 | 0.953 | 0.05 | R |
| 14 | PX$_{flank}$ | 9213−1 | GC | 346 | Lp | GIF 3066 | 0.286 | 0.001 | 149.7 | 1.5 | 11.290 | 0.09 | R |
| 15 | PX$_{flank}$ | 9213−1 | GC | 380 | Lp | GIF 3073 | 0.636 | 0.002 | 148.3 | 2.9 | 209.721 | 2.28 | R |
| 16 | PX$_{top}$ | 14531−1 | GC | 13 | Lp | GIF 3054 | 0.071 | 0.001 | 148.4 | 1.5 | 0.352 | 0.02 | R |
| 17 | PX$_{top}$ | 14531−1 | GC | 98 | Lp | GIF 3055 | 0.210 | 0.001 | 150.1 | 1.5 | 4.227 | 0.03 | R |
| 18 | PX$_{top}$ | 14531−1 | GC | 320 | Lp | GIF 3056 | 0.213 | 0.001 | 150.6 | 1.5 | 9.319 | 0.04 | R |
| 19 | PX$_{top}$ | 14531−1 | GC | 434 | Lp | GIF 3057 | 0.787 | 0.001 | 150.9 | 1.5 | 8.859 | 0.06 | R |
| 20 | PX$_{flank}$ | 14532−2 | GC | 20 | Lp | GIF 3067 | 0.481 | 0.001 | 148.9 | 1.5 | 4.838 | 0.09 | R |
| 21 | PX$_{flank}$ | 14532−2 | GC | 43 | Lp | GIF 3068 | 0.262 | 0.001 | 149.8 | 1.5 | 5.571 | 0.04 | R |
| 22 | PX$_{flank}$ | 14532−2 | GC | 67 | Lp | GIF 3069 | 0.454 | 0.001 | 149.1 | 1.5 | 2.924 | 0.03 | R |

IUP: Institute of Environmental Physics (IUP, Heidelberg University, Germany).
GEOMAR (no labcode available): Helmholtz Centre for Ocean Research (GEOMAR, Kiel, Germany).
GIF: Laboratoire des Sciences du Climat et de l'Environnement (LSCE, Gif-sur-Yvette, France).

Helmholtz Centre for Ocean Research (GEOMAR, Kiel, Germany) using a multicollector (MC) ICP-MS (Fietzke et al., 2005), and at the Institute of Environmental Physics (IUP, Heidelberg, Germany) also using a MC-ICP-MS (Wefing et al., 2017). All coral fragments were chemically cleaned prior to the measurements by applying previously published procedures (Fietzke et al., 2005; Frank et al., 2004). For comparison with the AMS $^{14}$C coral ages, absolute U/Th dates are reported as ka BP (Table 4). In addition, previously published coral ages collected from various coral mounds of the Belgica CMP were compiled (n$_{Holocene}$= 20, n$_{pre-Holocene}$= 14; see Table S1 in the Supplementary Material; Eisele et al., 2008; Frank et al., 2011; Frank et al., 2005; Frank et al., 2009; Raddatz et al., 2014; Schröder-Ritzrau et al., 2005; van der Land et al., 2014) and jointly discussed with the newly obtained data presented in this study. For comparison published AMS $^{14}$C ages were re-calibrated according to the method described above.

### 3.2. X-ray fluorescence (XRF) measurements

The elemental distribution of the four off-mound sediment cores (Table 2) was analysed using an AVAATECH XRF Core Scanner at MARUM (University of Bremen, Germany), which is a system for the non-destructive logging of split sediment cores (Jansen et al., 1998). XRF data were collected every 2 cm down-core over a 1 cm$^2$ area with slit size of 10 × 12 mm using generator settings of 10 kV, a current intensity of 0.25 mA, and a sampling time of 20 s directly at the split core surface. The here reported data were acquired by a Canberra X-PIPS Silicon Drift Detector (SDD; Model SXD 15C-150−500) with 150eV X-ray resolution, the Canberra Digital Spectrum Analyzer DAS 1000, and an Oxford Instruments 50W XTF5011 X-Ray tube with rhodium (Rh) target material. Raw data spectra were processed by the analysis of X-ray spectra by Iterative

Least square software (WIN AXIL) package from Canberra Eurisys. The resulting data are elements in counts per second. For this study, the two elements Ca and Fe were used to calculate the Ca/(Ca+Fe)-ratio, which was applied to correlate the four off-mound cores.

### 3.3. AMS radiocarbon dating: off-mound sediment cores

Between two and four multi-species samples of planktonic foraminifera (sample weight: ~8−10 mg) were sampled at various core depths from each off-mound sediment core (Table 2). The samples were used for AMS $^{14}$C age determinations, which were performed at the Keck Carbon Cycle AMS Facility of the Earth System Science Department (University of California, Irvine, USA) and at the BETA Analytic (Miami, Florida, USA). The $^{14}$C ages of the off-mound cores were corrected for $^{13}$C and calibrated using the MARINE13 calibration curve (Reimer et al., 2013) of the CALIB7.1 software (Stuiver and Reimer, 1993) without any additional local reservoir age correction. All radiocarbon ages are reported as ka BP (Table 5).

## 4. Results

### 4.1. Cold-water coral ages

Thirty-one coral fragments used for AMS $^{14}$C dating reveal coral ages between ~0.2 and 8.5 ka BP (Table 3). Eighteen of the 22 calculated Uranium-series coral ages range between 0.3 and 11.3 ka BP, while only four ages are considerably older ranging between ~98 and 253 ka BP (Table 4). Hence, only four coral ages were added to the existing pre-Holocene age dataset (n= 14), which spreads overall a rather long time interval of ~435 kyr (range: 79−514 ka BP; Supplementary Material: Fig. S1). This avoids a further detailed

**Table 5**
AMS radiocarbon ($^{14}$C) dates determined on multi-species samples of planktonic foraminifera from four off-mound sediment cores. The AMS $^{14}$C ages were corrected for $^{13}$C and calibrated using the MARINE13 calibration curve (Reimer et al., 2013) of the CALIB7.1 software (Stuiver and Reimer, 1993) without any additional local reservoir age correction. Estimated sedimentation rates are supplemented. CD: core depth, CAR: calibrated age range, MPA: median probability age, SR: sedimentation rate, calCT: calculated age of core top (youngest preserved slope deposits; see text for explanation), calCB: calculated age of core bottom.

| Core-ID (water depth) | CD (cm) | Labcode | $^{14}$C age (ka BP) | 1σ (ka BP) | 2σ (95.4%) CAR (ka BP, P = AD 1950) | | MPA (ka BP) | SR (cm kyr$^{-1}$) | calCT (ka BP) | calCB (ka BP) |
|---|---|---|---|---|---|---|---|---|---|---|
| GeoB14504-1 | 0 | | | | | | | | 12.217 | |
| (740 m) | 8 | UCIAMS 145991 | 11.285 | 0.04 | 12.646 | 12.876 | 12.750 | – | | |
| | 68 | BETA 361013 | 15.280 | 0.06 | 17.901 | 18.282 | 18.084 | 11.3 | | |
| | 238 | BETA 361014 | 16.020 | 0.06 | 18.727 | 18.995 | 18.858 | 219.6 | | |
| | 488 | UCIAMS 145992 | 17.670 | 0.08 | 20.580 | 21.069 | 20.819 | 127.5 | | |
| | 499 | | | | | | | | | 20.912 |
| GeoB14505-1 | 0 | | | | | | | | 18.300 | |
| (830 m) | 138 | BETA 361015 | 16.770 | 0.07 | 19.547 | 19.983 | 19.754 | – | | |
| | 323 | BETA 361016 | 18.140 | 0.07 | 21.197 | 21.753 | 21.475 | 107.5 | | |
| | 540 | | | | | | | | | 22.630 |
| GeoB14506-1 | 0 | | | | | | | | 20.530 | |
| (910 m) | 8 | UCIAMS 145993 | 17.450 | 0.08 | 20.307 | 20.806 | 20.560 | – | | |
| | 133 | BETA 361017 | 17.940 | 0.07 | 20.924 | 21.446 | 21.184 | 200.3 | | |
| | 533 | UCIAMS 145994 | 19.960 | 0.10 | 23.212 | 23.884 | 23.563 | 168.1 | | |
| | 550 | | | | | | | | | 23.651 |
| GeoB14507-1 | 0 | | | | | | | | 22.140 | |
| (990 m) | 8 | UCIAMS 145995 | 18.720 | 0.09 | 21.914 | 22.405 | 22.186 | – | | |
| | 278 | UCIAMS 145996 | 20.350 | 0.11 | 23.688 | 24.297 | 24.000 | 148.8 | | |
| | 476 | | | | | | | | | 25.038 |

BETA: BETA Analytic (Miami, Florida, USA).
UCIAMS: Keck Carbon Cycle AMS Facility of the Earth System Science Department (University of California, Irvine, USA).

discussion on short-term (centennial to millennial) variations in pre-Holocene mound formation. In contrast, 49 Holocene ages (<11.7 ka BP) were obtained during this study. Combined with 20 Holocene ages previously published for the Belgica CMP (Table 1), a total of 69 Holocene ages were used to interpret the Holocene development of the Belgica coral mounds.

All data reveal that CWCs started to re-colonise the Belgica CMP just after the onset of the Early Holocene at ~11.3 ka BP (Fig. 3), leading since then to a pronounced mound aggradation that lasts until today. All coral-bearing cores collected from the Belgica mounds lack preserved deposits of last glacial age (Supplementary Material: Table S1, Fig. S1), and most of them (nine out of 16 cores) reveal unconformities below their Holocene coral sequences separating these from previous Late Pleistocene coral-bearing sediments equivalent to Marine Isotope Stages (MIS) 5 or 7 (Supplementary Material: Table S1, Fig. S2). This is best displayed in one core from the deep Pollux mound (GeoB 14530-1), which displays a large unconformity between ~380 and 350 cm core depth, framed by corals of MIS 7 age (210 ka BP) and the afore-mentioned Early Holocene age (11.3 ka BP; Table 4). But also for a core collected from the shallow Lion's Head mound (GeoB14518-1), a Holocene sequence covering the last 8.6 kyr (Table 3) is directly underlain by very old (not datable) coral rubble deposits (Kremer, 2013).

By separating the Holocene ages obtained from corals of the shallow (n= 38; collected from nine on-mound cores and supplemented by four surface samples, depth range: 675–800 m) and deep mound chains (n= 31; collected from seven cores and two surface samples, depth range: 800–1000 m), it becomes clear that corals started to re-colonise the shallow mounds at ~8.6 ka BP, 2.7 kyr later compared to the deep mounds (Fig. 3). This temporal offset, calculated from the oldest Holocene coral age of the deep mound chain (Pollux Mound, core GeoB14530-1 sampled from ~950 m) and the oldest age of the shallow chain (Lion's Head Mound, core GeoB14518-1 sampled from ~700 m), ranges over a depth interval of ~250 m.

### 4.2. Off-mound core sediments

Age models for the four off-mound cores were established by AMS $^{14}$C ages in combination with core-to-core correlations of XRF-based Ca/(Ca+Fe)-ratios (Table 2). The AMS $^{14}$C ages obtained for all cores range between 12.8 and 24.0 ka BP (Table 5). Supplemented by the correlation of Ca/(Ca + Fe)-ratio data (ratios for all cores vary between 0.5 and 0.7), the off-mound cores encompass a total time interval of 12.2−25.0 ka BP (Fig. 4, Table 5). For the three deep cores (990-830 m water depth), only sediments of Last Glacial Maximum (LGM; 25-19 ka BP) age are preserved, while the shallowest core (740 m depth) also contains sediments as young as the Younger Dryas (YD; 12.9−11.7 ka BP; Fig. 4). Holocene sediments are missing in all cores. Our data further reveal that slope deposition ceased and/or erosion commenced at the core sites at different times (Fig. 5). While the deepest core (990 m water depth) preserves no sediments younger than 22.1 ka BP, the core tops of the shallower cores reveal progressively younger ages. The shallowest core (740 m depth) has a core top age of 12.2 ka BP, hence the resulting temporal offset in core top ages between the deep and shallow cores is ~10 kyr corresponding over a depth range of ~250 m (Fig. 4). Sedimentation rates during the LGM are high for all cores and range between 108 and 220 cm kyr$^{-1}$ (Table 5). For the shallowest core, the only core in which post-LGM sediments are preserved, the sedimentation rate significantly decreases to 11 cm kyr$^{-1}$ at around 18 ka BP (Table 5).

### 5. Discussion

Sedimentation patterns on continental slopes are significantly affected by turbulent energy, with the amount and persistence of the energy supplied controlling sedimentation processes such as erosion, transport and deposition (Stow et al., 2008). Accordingly, strong and persistent bottom currents are capable of forming thick and extensive accumulations of sediments (Hanebuth et al., 2015; Hernández-Molina et al., 2014; Rebesco et al., 2014; Stow et al., 2008), while even stronger bottom currents can prevent the
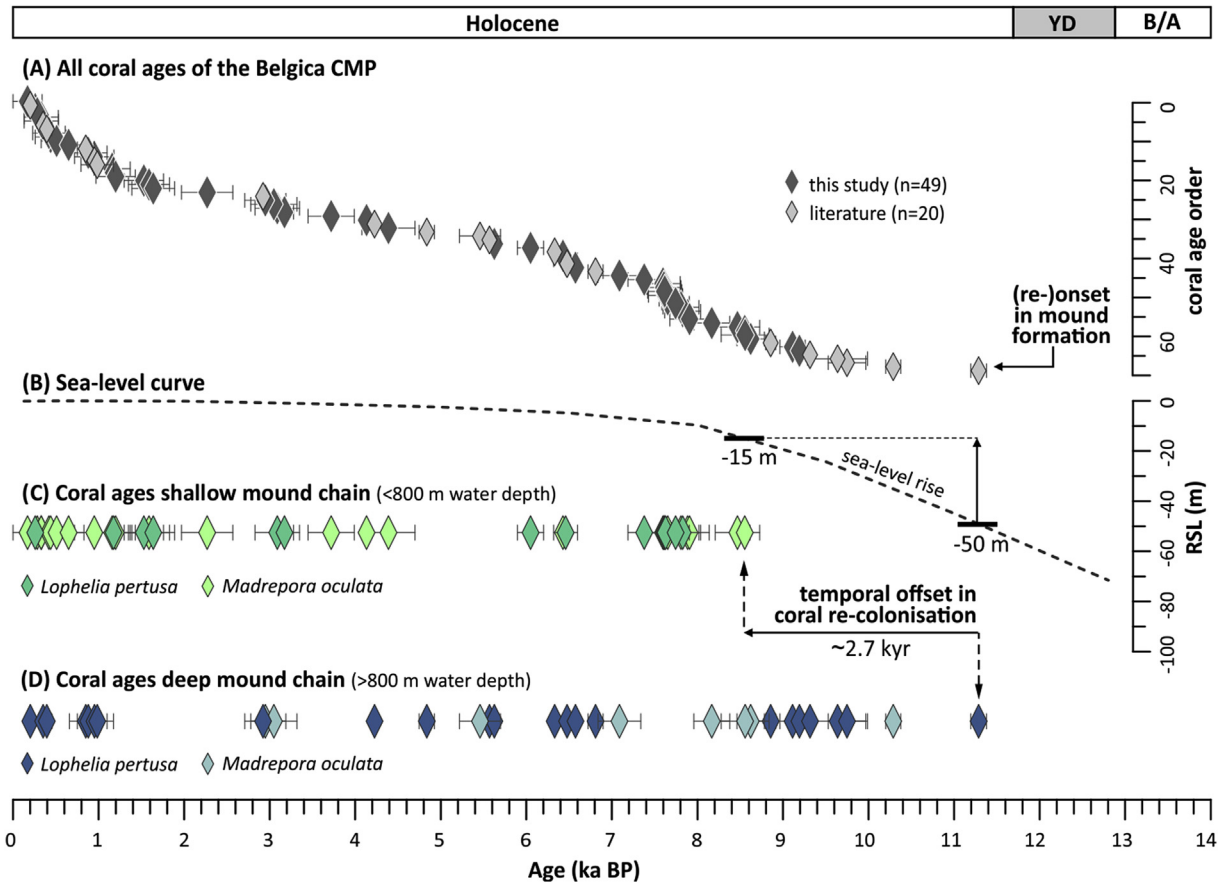
**Fig. 3.** Compilation of Holocene cold-water coral ages (<11.7 ka BP) from coral mounds of the Belgica coral mound province (CMP; Eisele et al., 2008; Frank et al., 2005, 2009, 2011; Raddatz et al., 2014; Schröder-Ritzrau et al., 2005; Van der Land et al., 2014; this study). (A) Chronological order of all coral ages (n= 69; dark grey diamonds: this study; light grey diamonds: literature). (B) Relative sea level (RSL) curve (Waelbroeck et al., 2002). (C) Ages (n= 38) of coral fragments collected from the shallow coral mound chain in water depths between 675 and 800 m (dark green diamonds: *Lophelia pertusa*; light green diamonds: *Madrepora oculata*), and (D) Ages (n= 31) obtained from coral fragments collected from the deep coral mound chain in water depths between 800 and 1000 m (dark blue diamonds: *L. pertusa*; light blue diamonds: *M. oculata*). The data reveal a depth-depending start of re-colonisation by corals indicated by a temporal offset of ~2.7 kyr between the shallow and deep coral mounds concurrent to a sea-level rise of about 35 m. (For interpretation of the references to colour in this figure legend, the reader is referred to the Web version of this article.)

deposition or cause the localised erosion of slope sediments (e.g., García et al., 2009; Hernández-Molina et al., 2008). High turbulent energy is mainly provided by geostrophic currents flowing parallel to the slope, and are further enhanced by internal waves inducing both contour-parallel and up- and down-slope currents (Cacchione et al., 2002; Pomar et al., 2012). The Belgica CMP on the eastern slope of the Porcupine Seabight widely exhibits large-scale depositional and erosional features and further provided the first clear observation of a co-occurrence of contourite drifts and coral mounds (Hebbeln et al., 2016; Van Rooij et al., 2003). Any sedimentary process on the slope (deposition, erosion, coral mound formation) is controlled by changes in turbulent energy supply, which are closely related to the climate-driven variability of the MOW acting as contour current (De Mol et al., 2005; Dorschel et al., 2005; Huvenne et al., 2002; Khélifi et al., 2014; Van Rooij et al., 2003, 2009), and the development of a TZ between the MOW and the overlying ENAW supporting internal waves and tides (e.g., Huvenne et al., 2009; Raddatz et al., 2014; Titschack et al., 2009). By combining palaeo-records obtained from the Belgica coral mounds and adjacent (off-mound) slope sediments, it is demonstrated that the observed depth-dependent pattern in slope sedimentation and coral mound formation was most likely controlled by millennial-scale changes in the intermediate water-mass dynamics linked to the last glacial termination.

All off-mound cores collected from the open continental slope had high sedimentation rates of 110−220 cm kyr$^{-1}$ during the LGM (Table 5). In conjunction with overall fine-grained sediments being deposited during this time, this points to rather low (or sluggish) energetic conditions prevailing at the eastern slope of the Porcupine Seabight (Fig. 6A). This is likely related to the absence of MOW influence, whose extent was confined to the Gulf of Cádiz during cold periods not affecting any margin further north (Kaboth et al., 2016; Petrovic et al., 2019; Stumpf et al., 2010; Toucanne et al., 2007; Voelker et al., 2006). During the last deglaciation, the MOW significantly strengthened and started to flow northwards between 600 and 1000 m water depths along the NE Atlantic margin (Rogerson et al., 2012b; Schönfeld and Zahn, 2000). For the Iberian slope, a first rapid increase in the upper MOW flow velocity is interpreted at 18 ka BP (Schönfeld and Zahn, 2000), and bottom currents further intensified at ~16 ka BP (see also Hanebuth et al., 2015). Our off-mound records from the eastern slope of the Porcupine Seabight reveal that also this northern area became influenced by more intense bottom currents after the LGM, related to the re-introduction of the MOW to the area (Fig. 6B). The old ages of the core tops (Table 5) indicate that the slope was subject to either non-deposition or sediment erosion. Such conditions would explain (i) the lack of Holocene sediments at all depths between 740 and 990 m; (ii) the lower sedimentation rate of 11 cm kyr$^{-1}$
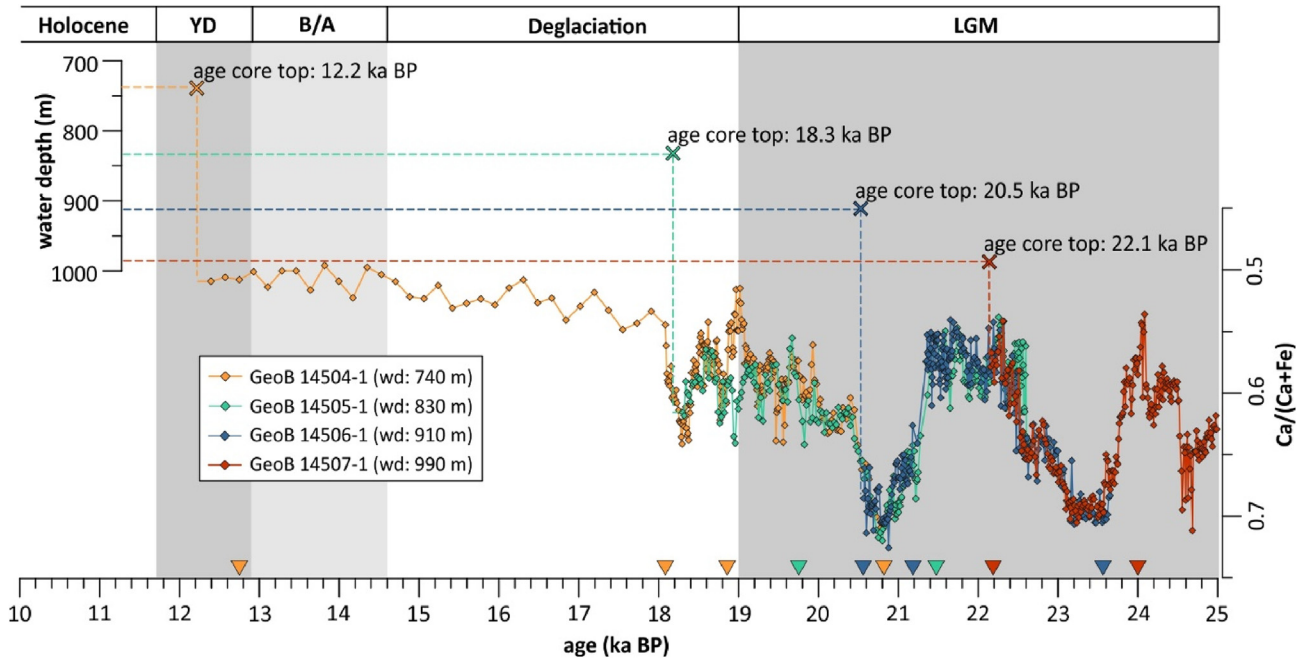
**Fig. 4.** Off-mound core records collected from the eastern slope of the Porcupine Seabight. Correlation of the four off-mound cores is based on Ca/(Ca+Fe)-ratios and eleven AMS radiocarbon datings (indicated as triangles on the x-axis). A water depth-dependent pattern becomes obvious indicated by upslope decreasing ages of the core tops (from ~22 ka BP to 12 ka BP). At the deepest site (990 m water depth, wd), slope deposits are of Last Glacial Maximum (LGM) age, while 250 m further upslope (740 m) sediments of Younger Dryas (YD) age are still preserved (B/A: Bølling-Allerød). Holocene sediments are completely missing for all the off-mound cores.
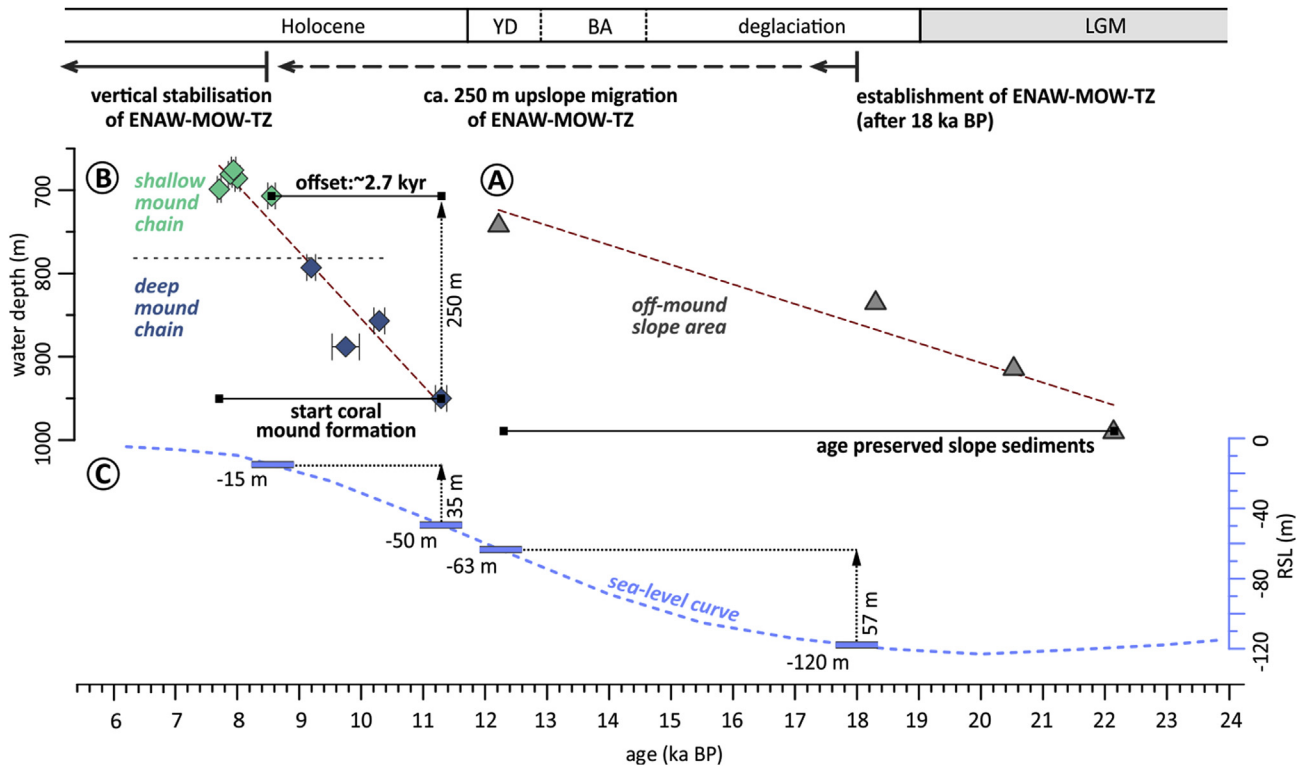


**Fig. 5.** Comparison between (A) water depth and the age of off-mound core tops (representing the youngest preserved slope sediments at the respective slope sites; grey triangles) across the eastern Porcupine Seabight (740–990 m water depth), and (B) water depth and the Holocene re-start of coral mound formation in the Belgica coral mound province, which reveals a temporal offset of ~2.7 kyr between the deep and shallow coral mound chains (note: only the oldest (available) Holocene coral ages obtained for the deep (blue diamonds) and shallow mounds (green diamonds) are displayed encompassing a water-depth range of 700–950 m). Both depth-dependent patterns are related to an upslope migration (of ~250 m) of the highly turbulent transition zone (TZ) between the Mediterranean Outflow Water (MOW) and the overlying Eastern North Atlantic Water (ENAW). (C) Blued dashed line represents relative sea level (RSL) curve according to Waelbroeck et al. (2002). LGM: Last Glacial Maximum; BA: Bølling-Allerød, YD: Younger Dryas. (For interpretation of the references to colour in this figure legend, the reader is referred to the Web version of this article.)
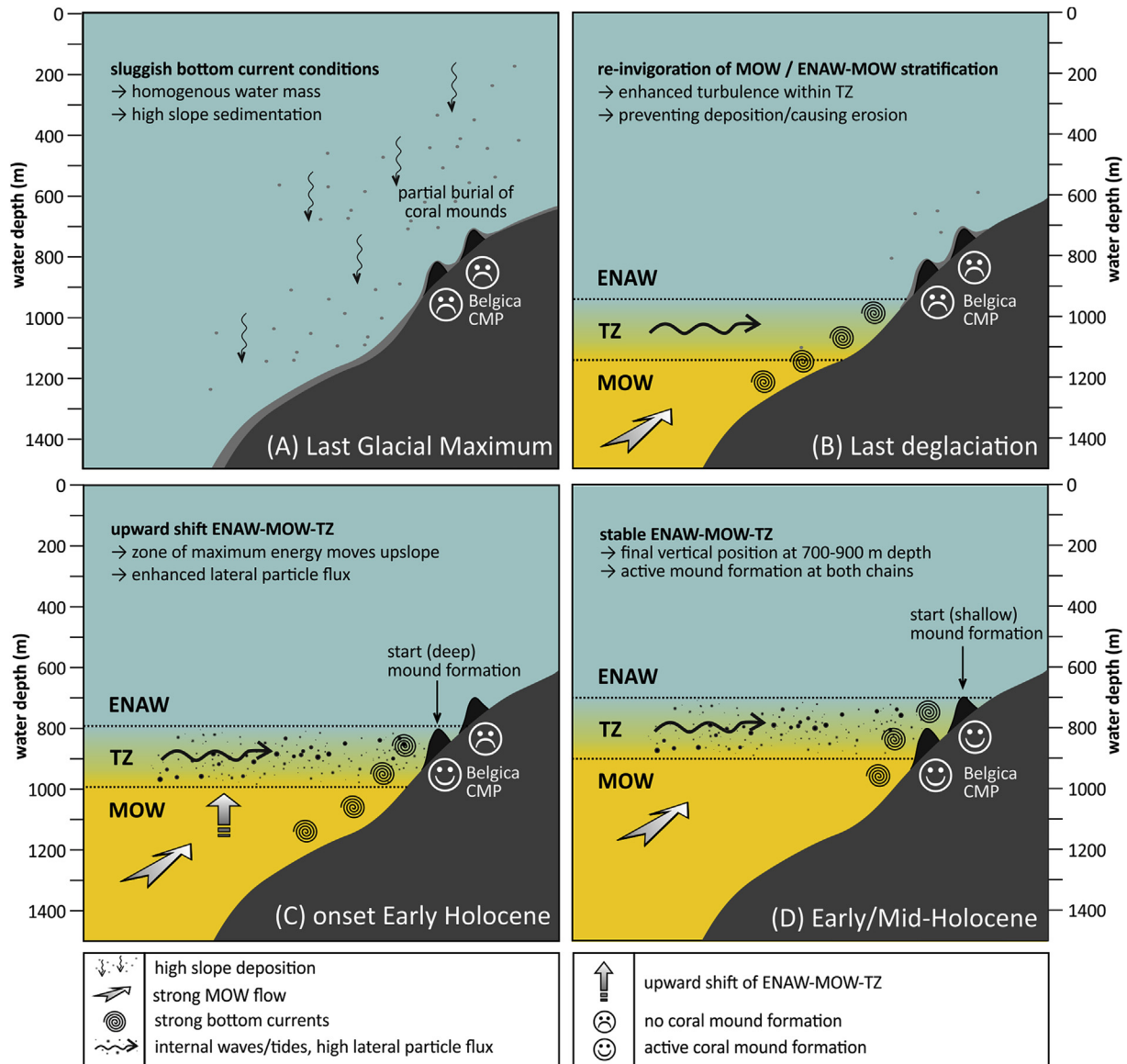
**Fig. 6.** Schematic model showing the chronology of slope sedimentation and coral mound formation within the Belgica coral mound province (CMP; Porcupine Seabight) in relation to oceanographic changes. (A) Last Glacial Maximum: Sluggish bottom current conditions prevailed causing a homogeneous water mass and high slope deposition. Coral-mound formation was inactive for the entire region. (B) Last deglaciation: A vigorous Mediterranean Outflow Water (MOW) flow re-established and a transition zone (TZ) between the MOW and the Eastern North Atlantic Water (ENAW) developed (after ~18 ka BP). Internal waves/tides propagating along the TZ cause high turbulence. The resulting accelerated bottom currents prevented deposition and/or caused erosion on the slope. Coral-mound formation was still inactive. (C) Onset Early Holocene: ENAW-MOW-TZ migrated continuously upward moving the zone of maximum energy and enhanced lateral supply of particulate material upslope. These conditions re-activated mound formation at the deep mound chain (at ~11.3 ka BP). (D) Mid/Early-Holocene: After an upslope migration of ~250 m, the ENAW-MOW-TZ reached its modern vertical position at 700−900 m depth and remained stable until today. The shallow coral mounds became finally influenced by the turbulent and trophic conditions of the TZ (at ~8.6 ka BP) and re-started their formation about 2.7 kyr later compared to the deep mounds.

between ~18-12 ka BP (though only preserved at the shallowest site at 740 m), which is an order of magnitude lower compared to the sedimentation rates during the LGM; and (iii) the downslope thinning of sediments deposited between ~22-18 ka BP (range of thickness of preserved sediments: ~5 m at 830 m water depth to zero at 990 m; Table 5, Fig. 4). Such large differences between adjacent sites (Fig. 1B) suggest erosion rather than non-deposition as the dominant process effecting all studied slope sites until today. However, the timing of the onset of erosion is not well constrained, although erosion is likely not to have commenced prior to ~18 ka BP, when a vigorous MOW re-established (Fig. 6B). Therefore, since the core top ages do not directly correspond to the onset of erosion, they are treated as possible maximum ages representing the

youngest preserved slope deposits (Fig. 5).

Nevertheless, the clear trend of the core top ages becoming progressively younger to shallower depths (from 22 ka BP at 990 m to 12 ka BP at 740 m; Table 5, Fig. 4) suggests a depth-related erosion onset, where the upslope decreasing ages of preserved slope deposits indicate the upward migration of conditions with maximum energy. Today, the high-energy zone is confined to the ENAW-MOW-TZ between 700 and 900 m depth (Fig. 2), where internal waves produce turbulence strong enough to cause erosion (e.g., Dorschel et al., 2007a). During the last deglaciation, when the MOW re-entered the Porcupine Seabight (after ~18 ka BP) and the ENAW-MOW-TZ became established, the zone of highest turbulent energy was likely at a deeper part of the slope compared to today

controlling erosion first on the deepest slope sites below 900 m (Fig. 6B), before it subsequently shifted upslope in a time-transgressive manner causing the delayed end of sedimentation and onset of erosion at the shallower slope sites (Figs. 5, 6C-D).

Independent evidence for vertical changes in the intermediate water-mass dynamics is provided by the Holocene coral age data of the Belgica mounds developing at the same water depth range (~680-1000 m; Table 1) as the corresponding off-mound cores (740−990 m; Table 2). The formation of coral mounds is positively influenced by internal waves propagating along the interface of intermediate water masses (e.g., Cyr et al., 2016). Internal waves cause the formation of nepheloid layers and enhance the lateral flux of fresh particulate organic matter, both increasing food availability for the CWCs thriving on mounds (Davies et al., 2009; Frederiksen et al., 1992; Hebbeln et al., 2016; Mienis et al., 2007, 2009; Mohn et al., 2014). In addition, internal waves increase the delivery of sediments that become deposited in the coral frame-work, and hence, support and maintain mound formation (Dorschel et al., 2005; Hebbeln et al., 2016; Titschack et al., 2009; Wienberg and Titschack, 2017). The close linkage between pres-ently active mound formation and increased turbulent energy associated to internal waves is proved by hydrographic measure-ments for various Atlantic CMPs (Davies et al., 2009; Hebbeln et al., 2014; Juva et al., 2020; Mienis et al., 2007; Mohn et al., 2014; White et al., 2007), while only few palaeo-records demonstrated this relationship also for past periods of mound formation (Matos et al., 2017; Wang et al., 2019), mainly due to a lack of an appropriate proxy to trace the effect of internal waves at palaeo-interfaces. Accordingly, Holocene re-initiation of mound formation in the Belgica CMP is likely due to the development of the ENAW-MOW-TZ and associated internal waves that induced turbulent and food-enriched conditions (Fig. 6C).

However, coral mound formation did not re-start prior to the Early Holocene (at ~11.3 ka BP for the deep mound chain), hence ~7 kyr later compared to the onset of erosion in the adjacent slope area, which already commenced during the deglaciation (Fig. 5A-B), when the ENAW-MOW-TZ was re-introduced to the Porcupine area. It is not clear what has caused the temporal delay between the onset in slope erosion and re-start in mound formation, but it is likely that a renewed colonisation by CWCs required further envi-ronmental preconditions than just an increase in turbulence and food supply. With respect to the high LGM sedimentation rates observed in the adjacent slope area (~110−220 cm kyr$^{-1}$; Table 5), it is possible that the Belgica mounds were also covered by glacial hemipelagic sediments, even though no glacial deposits are pre-served in the mound records (see also Dorschel et al., 2005; Eisele et al., 2008; Rüggeberg et al., 2007). This glacial sediment layer was probably less thick, as the elevated position of the mounds caused locally increased bottom-current strength even under overall sluggish current conditions (see Cyr et al., 2016; Mohn et al., 2014), and hence diminished the on-mound deposition of fine-grained sediments. Nevertheless, any glacial sediments potentially depos-ited on-mound had to be eroded, before coral rubble deposits of former mound formation periods became exposed and offered a hard substrate allowing for the settlement of new generations of coral larvae (Roberts et al., 2006).

Similar to the observed depth-dependent pattern in slope erosion, the Holocene coral age data also reveal a depth-related, step-wise reactivation in mound formation, as it started first at ~950 m at ~11.3 ka BP and about 2.7 kyr later at ~700 m water depth at ~8.6 ka BP (Fig. 5A-B), and hence, provides further evidence for an upward shift of the ENAW-MOW-TZ (Fig. 6C-D). By combining the data provided by both archives, slope sediments and coral mounds, it seems that the zone of highest turbulent energy within the ENAW-MOW-TZ migrated ~250 m upslope from ~990 to 950 m

to ~740-700 m water depth. This upslope shift of the ENAW-MOW-TZ is temporally framed by the onset of slope erosion concurrent to the invigoration of the MOW in the Porcupine Seabight at ~18 ka BP and the re-initiation of mound formation of the shallow Belgica mounds at 8.6 ka BP (Fig. 5A). The latter event also perfectly matches the time when the modern flow pattern of the MOW (flow depth and intensity), and hence, a stable intermediate water-mass stratification became finally established (8.3−6.8 ka BP; Schönfeld and Zahn, 2000; Stumpf et al., 2010). Until today, highly turbulent bottom-current conditions prevail in the Belgica CMP on the eastern slope of the Porcupine Seabight, which caused a continuous coral mound formation at both mound chains (with Holocene mean mound aggradation rates of 11-30 cm kyr$^{-1}$; see Supplementary Material: Fig. S3) and prevented deposition on the adjacent slope areas during the Mid- and Late Holocene (Fig. 6D).

Vertical shifts of the MOW (and associated interfaces) as observed for the Belgica CMP, are also reported from other sites in the NE Atlantic. A study from the Gulf of Cádiz showed a clear indication for a vertical shift of the MOW from the upper to the middle slope during the last glacial (Kaboth et al., 2016). A study from the western Iberian margin indicated an upward migration of the TZ between the MOW and the underlying LSW by about 80 m during the last deglaciation and the Early Holocene (~13.3 and 9.9 ka BP), which was explained by an overall shallowing of the MOW or vertical contraction of this water mass (Petrovic et al., 2019). A modelling study even suggested that the deglacial MOW-LSW-TZ was about 300 m deeper compared to today (Hanebuth et al., 2015). All these studies concluded that the vertical displacement of the MOW and hence the up- or downslope shift of turbulent conditions had a significant impact on the slope architecture by controlling large contourite systems. Studies from other ocean re-gions showing the direct consequence of the vertical displacement of water-mass boundaries on mound formation are comparably rare. However, a recent study from the Mauritanian CMP showed similar depth-related millennial-scale variations in mound devel-opment as we observed for the Belgica CMP. Off Mauritania, coral mounds are also arranged in two slope-parallel chains and their last glacial formation ceased in shallow water depths much earlier than in deeper waters (Wienberg et al., 2018). This was explained as a consequence of vertical changes in the intermediate water-mass structure that placed the mounds near or out of oxygen-depleted waters (Wienberg et al., 2018).

Finally, we can only speculate which process triggered the ver-tical shift of the ENAW-MOW-TZ at the eastern slope of the Por-cupine Seabight. Its upslope migration of ~250 m, which is best expressed by the depth-related delayed re-activation in mound formation during the Early Holocene, cannot solely be explained by the contemporaneous sea-level rise of ~35 m (Fig. 5C; Waelbroeck et al., 2002). Instead, the observed upslope shift might be related to a strengthening of the North Atlantic Deep Water (NADW), which from a minimum during the LGM, began to strengthen between 18 and 17 ka BP (e.g., Piotrowski et al., 2004). The increasing influence of the NADW might have forced the upward shift of the overlying intermediate water masses, and hence, of the associated turbulent conditions at their interfaces. In addition, a shift of the MOW flow to shallower depths, and hence a shoaling of the zone of maximum current activity, might be the result of a decrease in MOW density as a consequence of the deglacial warming and freshening of the Mediterranean Sea (Schönfeld and Zahn, 2000). Another explana-tion for a vertical displacement of intermediate water masses might be deduced from variations in the mid-depth ocean circulation in the NE Atlantic. An eastward extension of the sub-polar gyre, related to a northward displacement of the westerly winds over the North Atlantic at the transition from glacial to interglacial

conditions, resulted in its greater influence on the mid-depth water-mass structure in the semi-enclosed Porcupine basin (Colin et al., 2010; Montero-Serrano et al., 2011).

## 6. Conclusions

Internal waves associated with the transition zone between intermediate water masses of different densities significantly contribute to the supply of turbulent energy and particle flux. Consequently, they have a strong impact on slope sedimentation and habitats as they steer depositional/erosional processes and support marine ecosystems at mid-depths (~200-1000 m). This study of palaeo-records from coral mounds and adjacent slope sediments of the eastern slope (>1000 m) of the Porcupine Seabight shows their great potential to provide important archives for past intermediate water-mass hydrodynamic variations.

The deglacial invigoration of the MOW acting as a strong contour current along the slope was accompanied by the development of an ENAW-MOW-TZ. This invoked highly turbulent bottom-current conditions that induced the erosion of (glacial) slope sediments after ~18 ka BP and prevented deposition until today. These highly dynamic conditions supporting an increased lateral food and sediment flux also controlled the re-initiation of coral mound formation in the Belgica CMP, even though mound formation had not commenced prior the onset of the Early Holocene at ~11.3 ka BP. Moreover, the non-synchronous Holocene re-activation in mound formation identified for the Belgica CMP, indicated by a temporal offset of ~2.7 kyr between the deep and shallow mounds, provides further evidence for the partly large temporal variability in mound formation within one CMP.

A key conclusion to this work is the recognition of distinctive depth-dependent patterns observed for slope sedimentation and coral mound formation. Records of the onset of slope erosion and the re-activation in mound formation preserves distinct temporal delays between deep and shallow slope sites/mounds related to an upslope shift of the ENAW-MOW-TZ. Since the last deglaciation, this zone of maximum energy supply shallowed by ~250 m upslope over ~9–10 kyr, caused by 35 m seal-level rise combined with an oceanographic reorganization of the intermediate water masses, before the intermediate water-mass stratification became vertically stable during the Early/Mid-Holocene.

## Author statement

Claudia Wienberg: led the writing of the manuscript and conceived the study with Jürgen Titschack and Dierk Hebbeln. Claudia Wienberg and Dierk Hebbeln: further coordinated the scientific cruises and sediment/core sampling. Norbert Frank, Jan Fietzke and Ricardo De Pol-Holz: provided support in data collection (U/Th and radiocarbon dating). Markus Eisele and Anne Kremer: supported the sample collection and preparation and the technical data analyses. All authors interpreted the results and contributed to the final version of the manuscript.

## Declaration of competing interest

None.

## Acknowledgements

## Appendix A. Supplementary data

Supplementary data to this article can be found online at https://doi.org/10.1016/j.quascirev.2020.106310.

## References

Addamo, A.M., Vertino, A., Stolarski, J., García-Jiménez, R., Taviani, M., Machordom, A., 2016. Merging scleractinian genera: the overwhelming genetic similarity between solitary Desmophyllum and colonial Lophelia. BMC Evol. Biol. 16, 108.

Andersen, M.B., Stirling, C.H., Zimmermann, B., Halliday, A.N., 2010. Precise determination of the open ocean $^{234}U/^{238}U$ composition. Geochemistry Geophysics Geosystems 11, Q12003.

Baringer, M.O.N., Price, J.F., 1999. A review of the physical oceanography of the Mediterranean outflow. Mar. Geol. 155, 63–82.

Beyer, A., Schenke, H.W., Klenke, M., Niederjasper, F., 2003. High resolution bathymetry of the eastern slope of the Porcupine Seabight. Mar. Geol. 198, 27–54.

Beyer, A., Schenke, H.W., Klenke, M., Niederjasper, F., 2006. Terrain model of the eastern slope of the Porcupine Seabight (50 m grid size). PANGAEA. https://doi.org/10.1594/PANGAEA.370808.

Bonneau, L., Colin, C., Pons-Branchu, E., Mienis, F., Tisnérat-Laborde, N., Blamart, D., Elliot, M., Collart, T., Frank, N., Foliot, L., Douville, E., 2018. Imprint of Holocene climate variability on cold-water coral reef growth at the SW Rockall Trough margin, NE Atlantic. G-cubed 19, 2437–2452.

Bower, A.S., Serra, N., Ambar, I., 2002. Structure of the mediterranean undercurrent and mediterranean water spreading around the southwestern Iberian Peninsula. J. Geophys. Res.: Oceans 107, 25-21-25-19.

Cacchione, D.A., Drake, D.E., 1986. Nepheloid layers and internal waves over continental shelves and slopes. Geo Mar. Lett. 6, 147–152.

Cacchione, D.A., Pratson, L.F., Ogston, A.S., 2002. The shaping of continental slopes by internal tides. Science 296, 724–727.

Colin, C., Frank, N., Copard, K., Douville, E., 2010. Neodymium isotopic composition of deep-sea corals from the NE Atlantic: implications for past hydrological changes during the Holocene. Quat. Sci. Rev. 29, 2509–2517.

Cyr, F., van Haren, H., Mienis, F., Duineveld, G., Bourgault, D., 2016. On the influence of cold-water coral mound size on flow hydrodynamics, and vice versa. Geophys. Res. Lett. 43, 775–783.

Davies, A.J., Duineveld, G., Lavaleye, M., Bergman, M.J., van Haren, H., Roberts, J.M., 2009. Downwelling and deep-water bottom currents as food supply mechanisms to the cold-water coral Lophelia pertusa (Scleractinia) at the Mingulay Reef Complex. Limnol. Oceanogr. 54, 620–629.

De Haas, H., Mienis, F., Frank, N., Richter, T.O., Steinbacher, R., de Stigter, H., van der Land, C., van Weering, T.C.E., 2009. Morphology and sedimentology of (clustered) cold-water coral mounds at the south Rockall Trough margins, NE Atlantic Ocean. Facies 55, 1–26.

De Mol, B., Henriet, J.-P., Canals, M., 2005. Development of coral banks in the Porcupine Seabight: do they have Mediterranean ancestors? In: Freiwald, A., Roberts, J.M. (Eds.), Cold-water Corals and Ecosystems. Springer, Heidelberg, pp. 515–533.

De Mol, B., Kozachenko, M., Wheeler, A.J., Alvares, H., Henriet, J.-P., Olu-Le Roy, K., 2007. Thérèse mound: a case study of coral bank development in the Belgica mound province, Porcupine Seabight. Earth Planet Sci. Lett. 96, 103–120.

De Mol, B., Van Rensbergen, P., Pillen, S., Van Herreweghe, K., Van Rooij, D., McDonnell, A., Huvenne, V.A.I., Ivanov, M., Swennen, R., Henriet, J.-P., 2002. Large deep-water coral banks in the Porcupine Basin, southwest of Ireland. Mar. Geol. 188, 193–231.

Dickson, R.R., McCave, I.N., 1986. Nepheloid layers on the continental slope west of Porcupine Bank. Deep Sea Res. 33.

Dorschel, B., Hebbeln, D., Foubert, A., White, M., Wheeler, A.J., 2007a. Hydrodynamics and cold-water coral facies distribution related to recent sedimentary processes at Galway Mound west of Ireland. Mar. Geol. 244, 184–195.

Dorschel, B., Hebbeln, D., Rüggeberg, A., Dullo, W.-C., 2005. Growth and erosion of a cold-water coral covered carbonate mound in the Northeast Atlantic during the Late Pleistocene and Holocene. Earth Planet Sci. Lett. 233, 33–44.

Dorschel, B., Hebbeln, D., Rüggeberg, A., Dullo, W.-C., 2007b. Carbonate budget of a cold-water coral carbonate mound: Propeller Mound, Porcupine Seabight. Int. J. Earth Sci. 96, 73–83.

Douville, E., Sallé, E., Frank, N., Eisele, M., Pons-branchu, E., Ayrault, S., 2010. Rapid and accurate Th-U dating on ancient carbonates using inductivity coupled plasma-quadrupole mass spectrometry. Chem. Geol. 272, 1–11.

Duineveld, G.C.A., Lavaleye, M.S.S., Bergman, M.J.N., De Stigter, H., Mienis, F., 2007. Trophic structure of a cold-water coral mound community (Rockall Bank, NE Atlantic) in relation to the near-bottom particle supply and current regime. Bull. Mar. Sci. 81, 449–467.

Dullo, W.-C., Flögel, S., Rüggeberg, A., 2008. Cold-water coral growth in relation to the hydrography of the Celtic and Nordic European continental margin. Mar. Ecol. Prog. Ser. 371, 165–176.

Eisele, M., Hebbeln, D., Wienberg, C., 2008. Growth history of a cold-water coral covered carbonate mound - Galway Mound, Porcupine Seabight, NE-Atlantic. Mar. Geol. 253, 160–169.

Erdem, Z., Schönfeld, J., Glock, N., Dengler, M., Mosch, T., Sommer, S., Elger, J., Eisenhauer, A., 2016. Peruvian sediments as recorders of an evolving hiatus for the last 22 thousand years. Quat. Sci. Rev. 137, 1–14.

Ferdelman, T.G., Kano, A., Williams, T., Henriet, J.P., Scientists, I.E., 2006. Proceedings of the IODP Expedition 307. Modern Carbonate Mounds: Porcupine Drilling. IODP Management International, Washington DC. https://doi.org/10.2204/iodp.proc.307.2006.

Fietzke, J., Liebetrau, V., Eisenhauer, A., Dullo, W.-C., 2005. Determination of uranium isotope ratios by multi-static MIC-ICP-MS: method and implementation for precise U- and Th-series isotope measurements. J. Anal. Atomic Spectrom. 20, 395–401.

Foubert, A., Beck, T., Wheeler, A.J., Opderbecke, J., Grehan, A., Klages, M., Thiede, J., Henriet, J.-P., 2005. The Polarstern ARK-XIX/3a shipboard party, 2005. New view of the Belgica mounds, Porcupine, NE Atlantic: preliminary results from the Polarstern ARK-XIX/3a ROV cruise. In: Freiwald, A., Roberts, J.M. (Eds.), Cold-water Corals and Ecosystems. Springer, Heidelberg, pp. 403–415.

Foubert, A., Huvenne, V.A.I., Wheeler, A., Kozachenko, M., Opderbecke, J., Henriet, J.P., 2011. The Moira Mounds, small cold-water coral mounds in the Porcupine Seabight, NE Atlantic: Part B—evaluating the impact of sediment dynamics through high-resolution ROV-borne bathymetric mapping. Mar. Geol. 282, 65–78.

Frank, N., Freiwald, A., Lopez Correa, M., Wienberg, C., Eisele, M., Hebbeln, D., Van Rooij, D., Henriet, J.-P., Colin, C., van Weering, T., de Haas, H., Buhl-Mortensen, P., Roberts, J.M., De Mol, B., Douville, E., Blamart, D., Hatte, C., 2011. Northeastern Atlantic cold-water coral reefs and climate. Geology 39, 743–746.

Frank, N., Lutringer, A., Paterne, M., Blamart, D., Henriet, J.-P., van Rooij, D., van Weering, T.C.E., 2005. Deep-water corals of the northeastern Atlantic margin: carbonate mound evolution and upper intermediate water ventilation during the Holocene. In: Freiwald, A., Roberts, J.M. (Eds.), Cold-water Corals and Ecosystems. Springer, Heidelberg, pp. 113–133.

Frank, N., Paterne, M., Ayliffe, L., van Weering, T.C.E., Henriet, J.-P., Blamart, D., 2004. Eastern North Atlantic deep-sea corals: tracing upper intermediate water Δ14C during the Holocene. Earth Planet Sci. Lett. 219, 297–309.

Frank, N., Ricard, E., Lutringer-Paquet, A., van der Land, C., Colin, C., Blamart, D., Foubert, A., Van Rooij, D., Henriet, J.-P., de Haas, H., van Weering, T., 2009. The Holocene occurrence of cold water corals in the NE Atlantic: implications for coral carbonate mound evolution. Mar. Geol. 266, 129–142.

Frederiksen, R., Jensen, A., Westerberg, H., 1992. The distribution of the scleractinian coral *Lophelia pertusa* around the Faroe Islands and the relation to internal tidal mixing. Sarsia 77, 157–171.

García, M., Hernández-Molina, F.J., Llave, E., Stow, D.A.V., León, R., Fernández-Puga, M.C., Diaz del Río, V., Somoza, L., 2009. Contourite erosive features caused by the mediterranean outflow water in the Gulf of Cadiz: quaternary tectonic and oceanographic implications. Mar. Geol. 257, 24–40.

Hanebuth, T.J.J., Zhang, W., Hofmann, A.L., Löwemark, L.A., Schwenk, T., 2015. Oceanic density fronts steering bottom-current induced sedimentation deduced from a 50 ka contourite-drift record and numerical modeling (off NW Spain). Quat. Sci. Rev. 112, 207–225.

Hebbeln, D., Bender, M., Gaide, S., Titschack, J., Vandorpe, T., Van Rooij, D., Wintersteller, P., Wienberg, C., 2019a. Thousands of cold-water coral mounds along the Moroccan Atlantic continental margin: distribution and morphometry. Mar. Geol. 411, 51–61.

Hebbeln, D., da Costa Portilho-Ramos, R., Wienberg, C., Titschack, J., 2019b. The fate of cold-water corals in a changing world: a geological perspective. Front. Mar. Sci. 6.

Hebbeln, D., Van Rooij, D., Wienberg, C., 2016. Good neighbours shaped by vigorous currents: cold-water coral mounds and contourites in the North Atlantic. Mar. Geol. 378, 171–185.

Hebbeln, D., Wienberg, C., Wintersteller, P., Freiwald, A., Becker, M., Beuck, L., Dullo, C., Eberli, G.P., Glogowski, S., Matos, L., Forster, N., Reyes-Bonilla, H., Taviani, M., 2014. Environmental forcing of the Campeche cold-water coral province, southern Gulf of Mexico. Biogeosciences 11, 1799–1815.

Henry, L.-A., Frank, N., Hebbeln, D., Wienberg, C., Robinson, L., van de Flierdt, T., Dahl, M., Douarin, M., Morrison, C.L., López Correa, M., Rogers, A.D., Ruckelshausen, M., Roberts, J.M., 2014. Global ocean conveyor lowers extinction risk in the deep sea. Deep Sea Res. Part I 88, 8–16.

Hernández-Molina, F.J., Llave, E., Preu, B., Ercilla, G., Fontan, A., Bruno, M., Serra, N., Gomiz, J.J., Brackenridge, R.E., Sierro, F.J., Stow, D.A.V., García, M., Juan, C., Sandoval, N., Arnaiz, A., 2014. Contourite processes associated with the mediterranean outflow water after its exit from the Strait of Gibraltar: global and conceptual implications. Geology 42, 227–230.

Hernández-Molina, F.J., Stow, D.A.V., Llave, E., 2008. Continental slope contourites. In: Rebesco, M., Camerlenghi, A. (Eds.), Contourites. Developments in Sedimentology, 60. Elsevier, Amsterdam, pp. 379–408.

Huthnance, J.M., 1986. The Rockall slope current and shelf-edge processes. Proc. Roy. Soc. Edinburgh 88B, 83–101.

Huvenne, V.A.I., Bailey, W.R., Shannon, P.M., Naeth, J., di Primio, R., Henriet, J.-P., Horsfield, B., de Haas, H., Wheeler, A.J., Olu-Le Roy, K., 2007. The Magellan mound province in the Porcupine basin. Int. J. Earth Sci. 96, 85–101.

Huvenne, V.A.I., Beyer, A., de Haas, H., Dekindt, K., Henriet, J.-P., Kozachenko, M., Olu-Le Roy, K., Wheeler, A.J., the TOBI/Pelagia 197 and CARACOLE cruise participants, 2005. The seabed appearance of different coral bank provinces in the Porcupine Seabight, NE Atlantic: results from sidescan sonar and ROV seabed mapping. In: Freiwald, A., Roberts, J.M. (Eds.), Cold-water Corals and Ecosystems. Springer, Heidelberg, pp. 535–569.

Huvenne, V.A.I., Blondel, P., Henriet, J.-P., 2002. Textural analyses of sidescan sonar imagery from two mound provinces in the Porcupine Seabight. Mar. Geol. 189, 323–341.

Huvenne, V.A.I., Van Rooij, D., De Mol, B., Thierens, M., O'Donnell, R., Foubert, A., 2009. Sediment dynamics and palaeo-environmental context at key stages in the Challenger cold-water coral mound formation: clues from sediment deposits at the mound base. Deep Sea Res. Part I 56, 2263–2280.

Jansen, J.H.F., Van der Gaast, S.J., Koster, B., Vaars, A.J., 1998. CORTEX, a shipboard XRF-scanner for element analyses in split sediment cores. Mar. Geol. 151, 143–153.

Johnson, J., Ambar, I., Serra, N., Stevens, I., 2002. Comparative studies of the spreading of mediterranean water through the Gulf of Cadiz. Deep Sea Res. Part II Top. Stud. Oceanogr. 49, 4179–4193.

Juva, K., Flögel, S., Karstensen, J., Linke, P., Dullo, W.-C., 2020. Tidal dynamics control on cold-water coral growth: a high-resolution multivariable study on eastern Atlantic cold-water coral sites. Front. Mar. Sci. 7, 132.

Kaboth, S., Bahr, A., Reichart, G.-J., Jacobs, B., Lourens, L.J., 2016. New insights into upper MOW variability over the last 150kyr from IODP 339 Site U1386 in the Gulf of Cadiz. Mar. Geol. 377, 136–145.

Integrated Ocean Drilling Program Expedition 307 Scientists Kano, A., Ferdelman, T.G., Williams, T., Henriet, J.-P., Ishikawa, T., Kawagoe, N., Takashima, C., Kakizaki, Y., Abe, K., Sakai, S., Browning, E.L., Li, X., 2007. Age constraints on the origin and growth history of a deep-water coral mound in the northeast Atlantic drilled during Integrated Ocean Drilling Program Expedition 307. Geology 35, 1051–1054.

Khélifi, N., Sarnthein, M., Frank, M., Andersen, N., Garbe-Schönberg, D., 2014. Late Pliocene variations of the mediterranean outflow. Mar. Geol. 357, 182–194.

Kremer, A., 2013. Cold-water Coral Mound Carbonate Accumulation Rates from the Belgica Mound Province, Porcupine Seabight, SW off Ireland.. Master Thesis Department of Geosciences. University of Bremen, Bremen, Germany, p. 63.

Lim, A., Huvenne, V.A.I., Vertino, A., Spezzaferri, S., Wheeler, A.J., 2018. New insights on coral mound development from groundtruthed high-resolution ROV-mounted multibeam imaging. Mar. Geol. 403, 225–237.

Lim, A., Wheeler, A.J., Arnaubec, A., 2017. High-resolution facies zonation within a cold-water coral mound: the case of the Piddington Mound, Porcupine Seabight, NE Atlantic. Mar. Geol. 390, 120–130.

Lim, K., Ivey, G.N., Jones, N.L., 2010. Experiments on the generation of internal waves over continental shelf topography. J. Fluid Mech. 663, 385–400.

Locarnini, R.A., Mishonov, A.V., Antonov, J.I., Boyer, T.P., Garcia, H.E., Baranova, O.K., Zweng, M.M., Paver, C.R., Reagan, J.R., Johnson, D.R., Hamilton, M., Seidov, D., Levitus, S., 2013. World ocean Atlas 2013. Volume 1: temperature. In: Levitus, S., Mishonov, A. (Eds.), NOAA Atlas NESDIS 74. National Oceanographic Data Center, Ocean Climate Laboratory United States, National Environmental Satellite Data Information Service.

López Correa, M., Montagna, P., Joseph, N., Rüggeberg, A., Fietzke, J., Flögel, S., Dorschel, B., Goldstein, S.L., Wheeler, A., Freiwald, A., 2012. Preboreal onset of cold-water coral growth beyond the Arctic Circle revealed by coupled radiocarbon and U-series dating and neodymium isotopes. Quat. Sci. Rev. 34, 24–43.

Lozier, M.S., Stewart, N.M., 2008. On the temporally varying northward penetration of Mediterranean Overflow Water and eastward penetration of Labrador Sea Water. J. Phys. Oceanogr. 38, 2097–2103.

Matos, L., Wienberg, C., Titschack, J., Schmiedl, G., Frank, N., Abrantes, F., Cunha, M.R., Hebbeln, D., 2017. Coral mound development at the Campeche cold-water coral province, southern Gulf of Mexico: implications of Antarctic Intermediate Water increased influence during interglacials. Mar. Geol. 392, 53–65.

Mienis, F., de Stigter, H.C., White, M., Duineveld, G., de Haas, H., van Weering, T.C.E., 2007. Hydrodynamic controls on cold-water coral growth and carbonate-mound development at the SW and SE Rockall Trough Margin, NE Atlantic Ocean. Deep Sea Res. Part I 54, 1655–1674.

Mienis, F., van der Land, C., de Stigter, H.C., van de Vorstenbosch, M., de Haas, H., Richter, T., van Weering, T.C.E., 2009. Sediment accumulation on a cold-water carbonate mound at the Southwest Rockall Trough margin. Mar. Geol. 265, 40–50.

Millot, C., 2014. Heterogeneities of in- and out-flows in the Mediterranean Sea. Prog. Oceanogr. 120, 254–278.

Mohn, C., Rengstorf, A., White, M., Duineveld, G., Mienis, F., Soetaert, K., Grehan, A., 2014. Linking benthic hydrodynamics and cold-water coral occurrences: a high-resolution model study at three cold-water coral provinces in the NE Atlantic. Prog. Oceanogr. 122, 92–104.

Monteiro, P.M.S., Nelson, G., van der Plas, A., Mabille, E., Bailey, G.W., Klingelhoeffer, E., 2005. Internal tide—shelf topography interactions as a forcing factor governing the large-scale distribution and burial fluxes of particulate organic matter (POM) in the Benguela upwelling system. Continent. Shelf Res. 25, 1864–1876.

Montero-Serrano, J.-C., Frank, N., Colin, C., Wienberg, C., Eisele, M., 2011. The climate influence on the mid-depth Northeast Atlantic gyres viewed by cold-water corals. Geophys. Res. Lett. 38.

Mosch, T., Sommer, S., Dengler, M., Noffke, A., Bohlen, L., Pfannkuche, O., Liebetrau, V., Wallmann, K., 2012. Factors influencing the distribution of epibenthic megafauna across the Peruvian oxygen minimum zone. Deep Sea Res. Oceanogr. Res. Pap. 68, 123–135.

Paillet, J., Arhan, M., McCartney, M.S., 1998. Spreading of Labrador Sea water in the Eastern North Atlantic. J. Geophys. Res.: Oceans 103, 10223–10239.

Petrovic, A., Lantzsch, H., Schwenk, T., Marquardt, J., Titschack, J., Hanebuth, T.J.J., 2019. Post-LGM upward shift of the Mediterranean Outflow Water recorded in a contourite drift off NW Spain. Mar. Geol. 407, 334–349.

Pingree, R.D., 1993. Flow of waters to the west of the British Isles and in the Bay of Biscay. Deep-Sea Res. Part I 40, 369–388.

Pingree, R.D., LeCann, B., 1990. Structure, strength and seasonality of the slope currents in the Bay of Biscay region. J. Mar. Biol. Assoc. UK 70, 857–885.

Piotrowski, A.M., Goldstein, S.L., Hemming, S.R., Fairbanks, R.G., 2004. Intensification and variability of ocean thermohaline circulation through the last deglaciation. Earth Planet Sci. Lett. 225, 205–220.

Pollard, R.T., Griffiths, M.J., Cunningham, S.A., Read, J.F., Perez, F.F., Rios, A.F., 1996. Vivaldi 1991 - a study of the formation, circulation and ventilation of Eastern North Atlantic water. Prog. Oceanogr. 37, 167–192.

Pomar, L., Morsilli, M., Hallock, P., Bádenas, B., 2012. Internal waves, an under-explored source of turbulence events in the sedimentary record. Earth Sci. Rev. 111, 56–81.

Raddatz, J., Rüggeberg, A., Liebetrau, V., Foubert, A., Hathorne, E.C., Fietzke, J., Eisenhauer, A., Dullo, W.-C., 2014. Environmental boundary conditions of cold-water coral mound growth over the last 3 million years in the Porcupine Seabight, Northeast Atlantic. Deep Sea Res. Part II 99, 227–236.

Ratmeyer, V., cruise participants, 2006. Report and preliminary results of RV METEOR cruise M61/3, Development of Carbonate Mounds along the Celtic Continental Margin, Cork-Ponta Delgada, June 04 - June 21 2004. Berichte aus dem Fachbereich Geowissenschaften der Universität Bremen. Department of Geosciences, Bremen University, Germany. No. 247.

Rebesco, M., Hernández-Molina, F.J., Van Rooij, D., Wåhlin, A., 2014. Contourites and associated sediments controlled by deep-water circulation processes: state-of-the-art and future considerations. Mar. Geol. 352, 111–154.

Reid, J.L., 1979. On the contribution of the Mediterranean Sea outflow to the Norwegian-Greenland sea. Deep sea research Part A. Oceanogr. Res. Pap. 26, 1199–1223.

Reimer, P., Bard, E., Bayliss, A., Beck, J., Blackwell, P., Bronk Ramsey, C., Buck, C., Cheng, H., Edwards, R., Friedrich, M., Grootes, P., Guilderson, T., Haflidason, H., Hajdas, I., Hatté, C., Heaton, T., Hogg, A., Hughen, K., Kaiser, K., Kromer, B., Manning, S., Niu, M., Reimer, R., Richards, D., Scott, E., Southon, J., Turney, C., van der Plicht, J., 2013. IntCal13 and MARINE13 radiocarbon age calibration curves 0-50000 years calBP. Radiocarbon 55, 1869–1887.

Rice, A.L., Billet, D.S.M., Thurston, M.H., Lampitt, R.S., 1991. The Institute of oceanographic Sciences biology programme in the porcupine Seabight: background and general introduction. J. Mar. Biol. Assoc. U. K. 71, 281–310.

Rice, A.L., Thurston, M.H., New, A.L., 1990. Dense aggregations of a hexactinellid sponge, *Pheronema carpenteri*, in the Porcupine Seabight (northeast Atlantic Ocean), and possible causes. Prog. Oceanogr. 24, 179–196.

Roberts, J.M., Wheeler, A.J., Freiwald, A., 2006. Reefs of the deep: the biology and geology of cold-water coral ecosystems. Science 312, 543–547.

Rogerson, M., Rohling, E.J., Bigg, G.R., Ramirez, J., 2012. Paleoceanography of the Atlantic-Mediterranean exchange: overview and first quantitative assessment of climatic forcing. Rev. Geophys. 50.

Rüggeberg, A., Dullo, W.-C., Dorschel, B., Hebbeln, D., 2007. Environmental changes and growth history of a cold-water carbonate mound (Propeller Mound, Porcupine Seabight). Int. J. Earth Sci. 96, 57–72.

Schönfeld, J., Zahn, R., 2000. Late Glacial to Holocene history of the Mediterranean Outflow. Evidence from benthic foraminiferal assemblages and stable isotopes at the Portuguese margin. Palaeogeogr. Palaeoclimatol. Palaeoecol. 159, 85–111.

Schröder-Ritzrau, A., Freiwald, A., Mangini, A., 2005. U/Th-dating of deep-water corals from the eastern North Atlantic and the western Mediterranean Sea. In: Freiwald, A., Roberts, J.M. (Eds.), Cold-water Corals and Ecosystems. Springer, Heidelberg, pp. 691–700.

Serra, N., Ambar, I., Boutov, D., 2010. Surface expression of Mediterranean Water dipoles and their contribution to the shelf/slope − open ocean exchange. Ocean Sci. 6, 191–209.

Shanmugam, G., 2017. Contourites: physical oceanography, process sedimentology, and petroleum geology. Petrol. Explor. Dev. 44, 183–216.

Stow, D.A.V., Hunter, S., Wilkinson, D., Hernández-Molina, F.J., 2008. Chapter 9 the nature of contourite deposition. In: Rebesco, M., Camerlenghi, A. (Eds.), Developments in Sedimentology. Elsevier, pp. 143–156.

Stuiver, M., Reimer, P.J., 1993. Extended $^{14}$C database and revised CALIB radiocarbon calibration program. Radiocarbon 35, 215–230.

Stumpf, R., Frank, M., Schönfeld, J., Haley, B.A., 2010. Late quaternary variability of mediterranean outflow water from radiogenic Nd and Pb isotopes. Quat. Sci. Rev. 29, 2462–2472.

Thierens, M., Browning, E., Pirlet, H., Loutre, M.F., Dorschel, B., Huvenne, V.A.I., Titschack, J., Colin, C., Foubert, A., Wheeler, A.J., 2013. Cold-water coral carbonate mounds as unique palaeo-archives: the Plio-Pleistocene Challenger Mound record (NE Atlantic). Quat. Sci. Rev. 73, 14–30.

Titschack, J., Thierens, M., Dorschel, B., Schulbert, C., Freiwald, A., Kano, A., Takashima, C., Kawagoe, N., Li, X., 2009. Carbonate budget of a cold-water coral mound (Challenger Mound, IODP Exp. 307). Mar. Geol. 259, 36–46.

Toucanne, S., Mulder, T., Schönfeld, J., Hanquiez, V., Gonthier, E., Duprat, J., Cremer, M., Zaragosi, S., 2007. Contourites of the Gulf of Cadiz: a high-resolution record of the paleocirculation of the Mediterranean outflow water during the last 50,000 years. Palaeogeogr. Palaeoclimatol. Palaeoecol. 246, 354–366.

van Aken, H.M., 2000. The hydrography of the mid-latitude Northeast Atlantic Ocean: II: the intermediate water masses. Deep Sea Res. Oceanogr. Res. Pap. 47, 789–824.

van Aken, H.M., Becker, G., 1996. Hydrography and through-flow in the North-Eastern North Atlantic Ocean: the NANSEN project. Prog. Oceanogr. 38, 297–346.

van der Land, C., Eisele, M., Mienis, F., de Haas, H., Hebbeln, D., Reijmer, J.J.G., van Weering, T.C.E., 2014. Carbonate mound development in contrasting settings on the Irish margin. Deep Sea Res. Part II 99, 297–306.

Van Rooij, D., De Mol, B., Huvenne, V.A.I., Ivanov, M., Henriet, J.P., 2003. Seismic evidence of current-controlled sedimentation in the Belgica mound province, upper Porcupine slope, southwest of Ireland. Mar. Geol. 195, 31–53.

Van Rooij, D., Huvenne, V.A.I., Blamart, D., Henriet, J.-P., Wheeler, A., de Haas, H., 2009. The Enya mounds: a lost mound-drift competition. Int. J. Earth Sci. 98, 849–863.

Vic, C., Naveira Garabato, A.C., Green, J.A.M., Waterhouse, A.F., Zhao, Z., Melet, A., de Lavergne, C., Buijsman, M.C., Stephenson, G.R., 2019. Deep-ocean mixing driven by small-scale internal tides. Nat. Commun. 10, 2099.

Victorero, L., Blamart, D., Pons-Branchu, E., Mavrogordato, M.N., Huvenne, V.A.I., 2016. Reconstrcution of the formation history of the Darwin Mounds, N Rockall Trough: how the dynamics of a sandy contourite affected cold-water coral growth. Mar. Geol. 378, 186–195.

Voelker, A.H.L., Lebreiro, S.M., Schönfeld, J., Cacho, I., Erlenkeuser, H., Abrantes, F., 2006. Mediterranean outflow strengthening during northern hemisphere coolings: a salt source for the glacial Atlantic? Earth Planet Sci. Lett. 245, 39–55.

Waelbroeck, C., Labeyrie, L., Michel, E., Duplessy, J.C., McManus, J.F., Lambeck, K., Balbon, E., Labracherie, M., 2002. Sea-level and deep water temperature changes derived from benthic foraminifera isotopic records. Quat. Sci. Rev. 21, 295–305.

Wang, H., Lo Iacono, C., Wienberg, C., Titschack, J., Hebbeln, D., 2019. Cold-water coral mounds in the southern Alboran Sea (western Mediterranean Sea): internal waves as an important driver for mound formation since the last deglaciation. Mar. Geol.

Wefing, A.-M., Arps, J., Blaser, P., Wienberg, C., Hebbeln, D., Frank, N., 2017. High precision U-series dating of scleractinian cold-water corals using an automated chromatographic U and Th extraction. Chem. Geol. 475, 140–148.

Wheeler, A.J., Beyer, A., Freiwald, A., de Haas, H., Huvenne, V.A.I., Kozachenko, M., Olu-Le Roy, K., Opderbecke, J., 2007. Morphology and environment of cold-water coral carbonate mounds on the NW European margin. Int. J. Earth Sci. 96, 37–56.

Wheeler, A.J., Kozachenko, M., Beyer, A., Foubert, A., Huvenne, V.A.I., Klages, M., Masson, D.G., Olu-Le Roy, K., Thiede, J., 2005. Sedimentary processes and carbonate mounds in the Belgica mound province, porcupine Seabight, NE Atlantic. In: Freiwald, A., Roberts, J.M. (Eds.), Cold-water Corals and Ecosystems. Springer, Heidelberg, pp. 571–603.

Wheeler, A.J., Kozachenko, M., Henry, L.A., Foubert, A., de Haas, H., Huvenne, V.A.I., Masson, D.G., Olu, K., 2011. The Moira Mounds, small cold-water coral banks in the Porcupine Seabight, NE Atlantic: Part A—an early stage growth phase for future coral carbonate mounds? Mar. Geol. 282, 53–64.

White, M., 2007. Benthic dynamics at the carbonate mound regions of the Porcupine Sea Bight continental margin. Int. J. Earth Sci. 96, 1–9.

White, M., Dorschel, B., 2010. The importance of the permanent thermocline to the cold-water coral carbonate mound distribution in the NE Atlantic. Earth Planet Sci. Lett. 296, 395–402.

White, M., Roberts, J.M., Van Weering, T.C.E., 2007. Do bottom-intensified diurnal tidal currents shape the alignement of carbonate mounds in the NE Atlantic? Geo Mar. Lett. 27, 391–397.

Wienberg, C., Beuck, L., Coughlan, M., Dimmler, W., Eisele, M.H., Freiwald, A., Klann, M., Ruhland, G., Stone, J., 2010. Report and preliminary results of RV POSEIDON cruise POS400, CORICON - Cold-water corals along the Irish continental margin, Vigo-Cork, June 29 - July 15 2010. Berichte aus dem Fachbereich Geowissenschaften der Universität Bremen. Department of Geosciences, Bremen University, Germany. No. 275.

Wienberg, C., Titschack, J., 2017. Framework-forming scleractinian cold-water corals through space and time: a late Quaternary North Atlantic perspective. In: Rossi, S., Bramanti, L., Gori, A., Orejas Saco del Valle, C. (Eds.), Marine Animal Forests: the Ecology of Benthic Biodiversity Hotspots. Springer, Cham, pp. 699–732.

Wienberg, C., Titschack, J., Freiwald, A., Frank, N., Lundälv, T., Taviani, M., Beuck, L., Schröder-Ritzrau, A., Krengel, T., Hebbeln, D., 2018. The giant Mauritanian cold-

water coral mound province: oxygen control on coral mound formation. Quat. Sci. Rev. 185, 135−152.

Williams, T., Kano, A., Ferdelman, T.G., Henriet, J.-P., Abe, K., Andres, M.S., Bjerager, M., Browning, E.L., Cragg, B.A., De Mol, B., Dorschel, B., Foubert, A., Frank, T.D., Fuwa, Y., Gharib, J.J., Gregg, J.M., Huvenne, V.A.I., Léonide, P., Li, X., Mangelsdorf, K., Tanaka, A., Monteys, F.X., Novosel, I., Sakai, S., Samarkin, V.A., Sasaki, K., Spivack, A.J., Takashima, C., Titschack, J., 2006. Cold-water coral

mounds revealed. EOS, Trans., Am. Geophys. Union 87, 525−526.

Zweng, M.M., Reagan, J.R., Antonov, J.I., Locarnini, R.A., Mishonov, A.V., Boyer, T.P., Garcia, H.E., Baranova, O.K., Johnson, D.R., Seidov, D., Biddle, M.M., Levitus, S., 2013. World ocean Atlas 2013. Volume 2: salinity. In: Levitus, S., Mishonov, A. (Eds.), NOAA Atlas NESDIS 74. National Oceanographic Data Center, Ocean Climate Laboratory United States, National Environmental Satellite Data Information Service, p. 39.